Geoelectric response and crustal electrical-conductivity structure of the Flin Flon Belt, Trans-Hudson Orogen, Canada[1]

I.J. Ferguson, Alan G. Jones, Yu Sheng, X. Wu, and I. Shiozaki

Abstract: A Lithoprobe magnetotelluric survey across the Palaeoproterozoic Trans-Hudson Orogen included 34 sites within the Flin Flon Belt and adjacent geological domains. The magnetotelluric impedance tensors and geomagnetic induction vectors reveal four distinct geoelectric zones along this segment of the Lithoprobe transect. In the east and west, the geoelectric responses are dominated by the contrast between intrusive rocks and more conductive ocean-floor assemblages. A significant characteristic of the responses throughout the Flin Flon Belt is the very strong galvanic distortion of the electric field, which reflects the complexity of the upper crustal geological structure in the greenstone belt, requiring careful application of distortion removal methods. The responses at sites near the north of the Flin Flon Belt are related to the boundary with the southern flank of the Kisseynew gneiss belt. To the south, at sites near Athapapuskow Lake, the responses are dominated by a strong upper-crustal conductor. The magnetotelluric observations show that the Athapapuskow Lake conductivity anomaly extends for at least 40 km along strike (~N36°E), and is roughly two-dimensional in form. Numerical modelling shows that the top of the body dips southeast at 20–50° from a western edge coincident with the Athapapuskow Lake shear zone. The conductor lies in the eastern part of the Namew gneiss complex. The magnetotelluric method cannot resolve the exact spatial distribution of conductive rocks but it is probable that the anomaly is caused by a series of isolated conductors (with resistivity <1 Ω·m) associated with subordinate graphitic and sulphidic supracrustal gneisses.

Résumé : Un relevé Lithoprobe à travers l'orogène Paléoprotérozoïque transhudsonien comprend 34 sites dans la ceinture de Flin Flon et autres domaines géologiques adjacents. Les tenseurs d'impédance magnétotellurique et les vecteurs d'induction géomagnétique révèlent quatre zones géoélectriques distinctes le long de ce segment du transect Lithoprobe. À l'est et à l'ouest, les réponses géoélectriques sont dominées par le contraste entres les roches intrusives et les assemblages plus conducteurs des fonds océaniques. Une caractéristique importante des réponses à travers la ceinture de Flin Flon est la très grande distorsion galvanique du champ électrique, ce qui reflète la complexité de la structure géologique de la croûte supérieure dans la ceinture de roches vertes et exige donc une application attentive des méthodes pour enlever la distorsion. Les réponses à des sites près du nord de la ceinture de Flin Flon sont reliées à la limite avec le flanc sud de la ceinture gneissique Kisseynew. Vers le sud, sur des sites à proximité du lac Athapapuskow, les réponses sont dominées par un fort conducteur dans la croûte supérieure. Les observations magnétotelluriques montrent que l'anomalie de conductivité du lac Athapapuskow s'étend pour au moins 40 km parallèlement à la direction (~N36°E) et qu'elle a une forme plus ou moins bi-dimensionnelle. Une modélisation numérique montre que la partie supérieure du corps a un pendage vers le sud-est de 20 à 50° à partir d'une bordure ouest qui coïncide avec la zone de cisaillement du lac Athapapuskow. Le conducteur se trouve dans la partie est du complexe gneissique de Namew. La méthode magnétotellurique ne peut résoudre la distribution spatiale exacte des roches conductrices mais il est probable que l'anomalie soit causée par une série de conducteurs isolés (résistivité <1 Ω·m) associés à des gneiss supracrustaux subordonnés, sulfurés et graphitiques.

[Traduit par la Rédaction]

Received January 28, 1999. Accepted November 25, 1999.

I.J. Ferguson and X. Wu. Department of Geological Sciences, University of Manitoba, Winnipeg, MB R3T 2N2, Canada.
A.G. Jones.[2] Geological Survey of Canada, 615 Booth Street, Ottawa, ON K1A 0E9, Canada.
Y. Sheng. Department of Earth Sciences, National Natural Sciences Foundation, Beijing 100083, China.
I. Shiozaki. Department of Civil Engineering, Tottori University, 4 – 101 Minami Koyama-cho, Tottori, Japan.

[1]Geological Survey of Canada Contribution 1998070; Lithoprobe Publication 1137.
[2]Corresponding author (e-mail: ajones@cg.nrcan.gc.ca).

Introduction

The lithospheric structure of the Trans-Hudson Orogen in northern Saskatchewan and Manitoba is being studied as part of the Canadian multidisciplinary Lithoprobe Project. The objectives of the Trans-Hudson Orogen Transect (THOT) investigations include delineation of internal geological domains, imaging of major faults and shear zones of the orogen, and definition of the margins with the bordering Archaean cratons (Clowes 1993). Approximately 200 magnetotelluric (MT) soundings have been completed as part of THOT activities since 1991, and in this paper we analyze and model a subset of this extensive dataset to determine and interpret the electrical conductivity structure of the Flin Flon Belt.

Fig. 1. Major geological divisions within the Trans-Hudson Orogen (modified from Lucas et al. 1994). The map also shows the locations of Lithoprobe seismic reflection profiles. FFB, Flin Flon Belt; GD, Glennie Domain; HLB, Hanson Lake Block; KD, Kisseynew Domain (Kisseynew gneiss belt); LRD, La Ronge Domain; RD, Rottenstone Domain; TF, Tabbernor fault; W, Archean windows; WB, Wathaman Batholith; WD, Wollaston Domain. The small box shows the area of the present study.

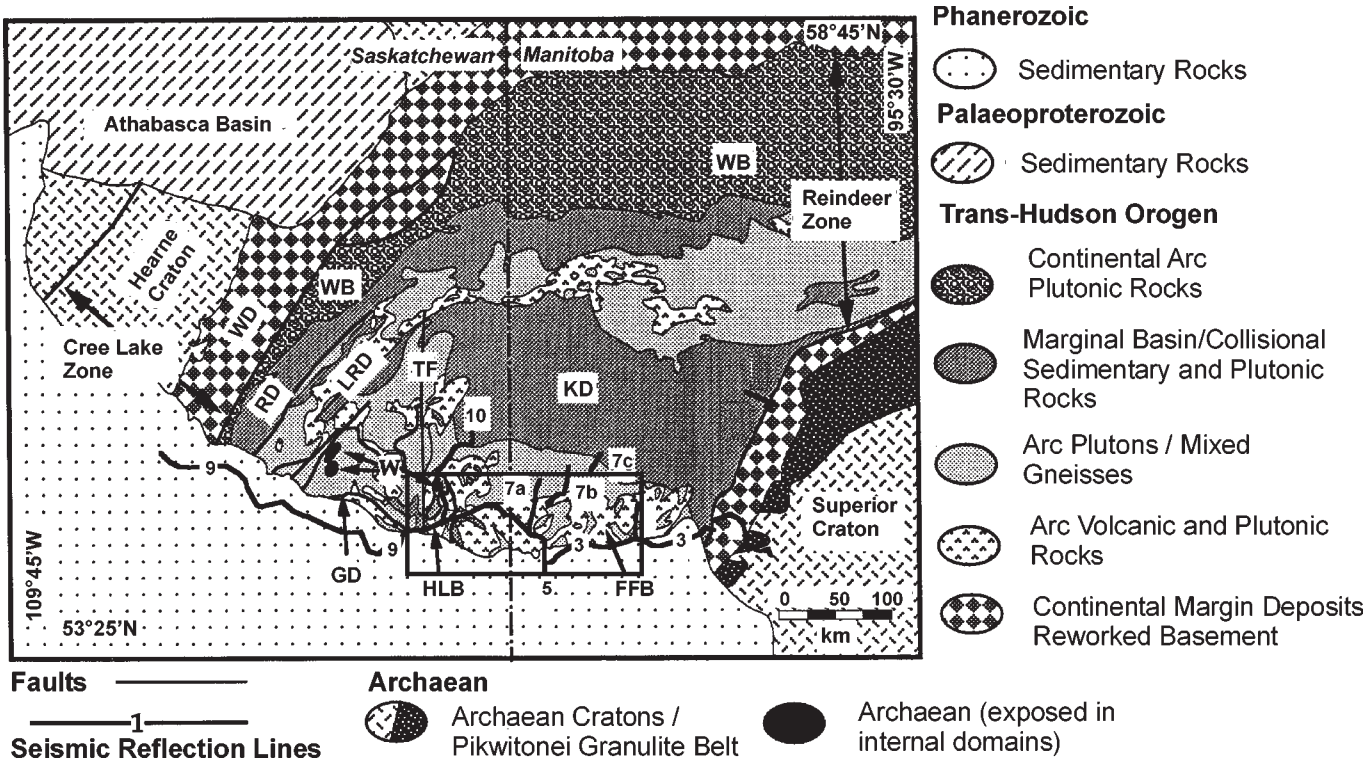

The Trans-Hudson Orogen (THO) is a Palaeoproterozoic orogenic belt forming part of a major North American system extending from South Dakota, across Hudson Bay, into Greenland and Labrador (Lewry and Collerson 1990), with possible counterparts in Scandinavia (Jones 1993). Within Canada, the orogen forms a 500 km wide region between the Superior Province to the southeast and the Hearne and Rae provinces in the north and northwest. The internal part of the orogen, the Reindeer Zone (Fig. 1), comprises ca. 1.9–1.8 Ga magmatic arc and sedimentary basin rocks accreted to the margins during successive arc–continent collisions prior to a terminal collision at ca. 1.8 Ga. The Flin Flon Belt comprises composite island-arc and back-arc assemblages and alluvial–fluvial sedimentary rocks.

Electromagnetic (EM) studies can contribute significantly to lithospheric investigations. In contrast to bulk physical properties, such as density, seismic velocity, and acoustic impedance measured by seismic and potential field methods, electrical conductivity is much more sensitive to minor geochemical constituents, including metallic sulphides, graphite, and fluids. Consequently, EM methods provide complementary, sometimes supportive but other times alternative, interpretations of geological units containing these constituents. EM results are particularly powerful when used to exclude hypotheses as part of joint interpretation. In general, EM methods, based on diffusive signal propagation, provide poorer spatial resolution than seismic methods and wave signal propagation. However in the case of near-vertical structures, including faults, shear zones, and contacts, EM methods can often provide superior resolution to seismic methods (e.g., Jones et al. 1992; Unsworth et al. 1997).

A number of crustal-scale EM studies have been completed within the THO, but no large-scale studies have been completed in the present study area prior to those described herein. Early geomagnetic studies in the orogen during the 1960s and early 1970s revealed the presence of a major continental-scale conductor, the North American Central Plains (NACP) conductivity anomaly, running north through the Dakotas and Saskatchewan (see brief historical review in Jones et al. 1997). Studies in the early 1980s demonstrated that the NACP turns east in northern Saskatchewan and crosses northern Manitoba to Hudson Bay. This anomaly was attributed to rocks associated with a Proterozoic collision zone extending from the southern Rockies to northern Canada before the extent of the THO was confirmed through potential field and basement core analysis (Camfield and Gough 1977).

Earlier papers have described analyses of the Lithoprobe MT data from various parts of the THO. Jones and Corriea (1992) described results from a preliminary survey in eastern Saskatchewan; Jones et al. (1993, 1996) described MT results from the NACP anomaly; Jones and Kalvey (1993) and Jones et al. (1996) described results from northern Saskatchewan; and White et al. (1996, 1997) described UTEM (University of Toronto electromagnetic system) survey results from the Thompson Belt in central Manitoba. Jones and

Fig. 2. Exposed and sub-Palaeozoic geology of the Flin Flon Belt showing MT sites used in this study. ALSZ, Athapapuskow Lake Shear Zone; BCF, Berry Creek Fault; ELSZ, Elbow Lake Shear Zone; NLS, Namew Lake Structure; SLF, Suggi Lake Fault; SRSZ, Spruce Rapids Shear Zone; TASZ, Tartan–Annabel Shear Zone. (Modified from Leclair et al. 1994.)

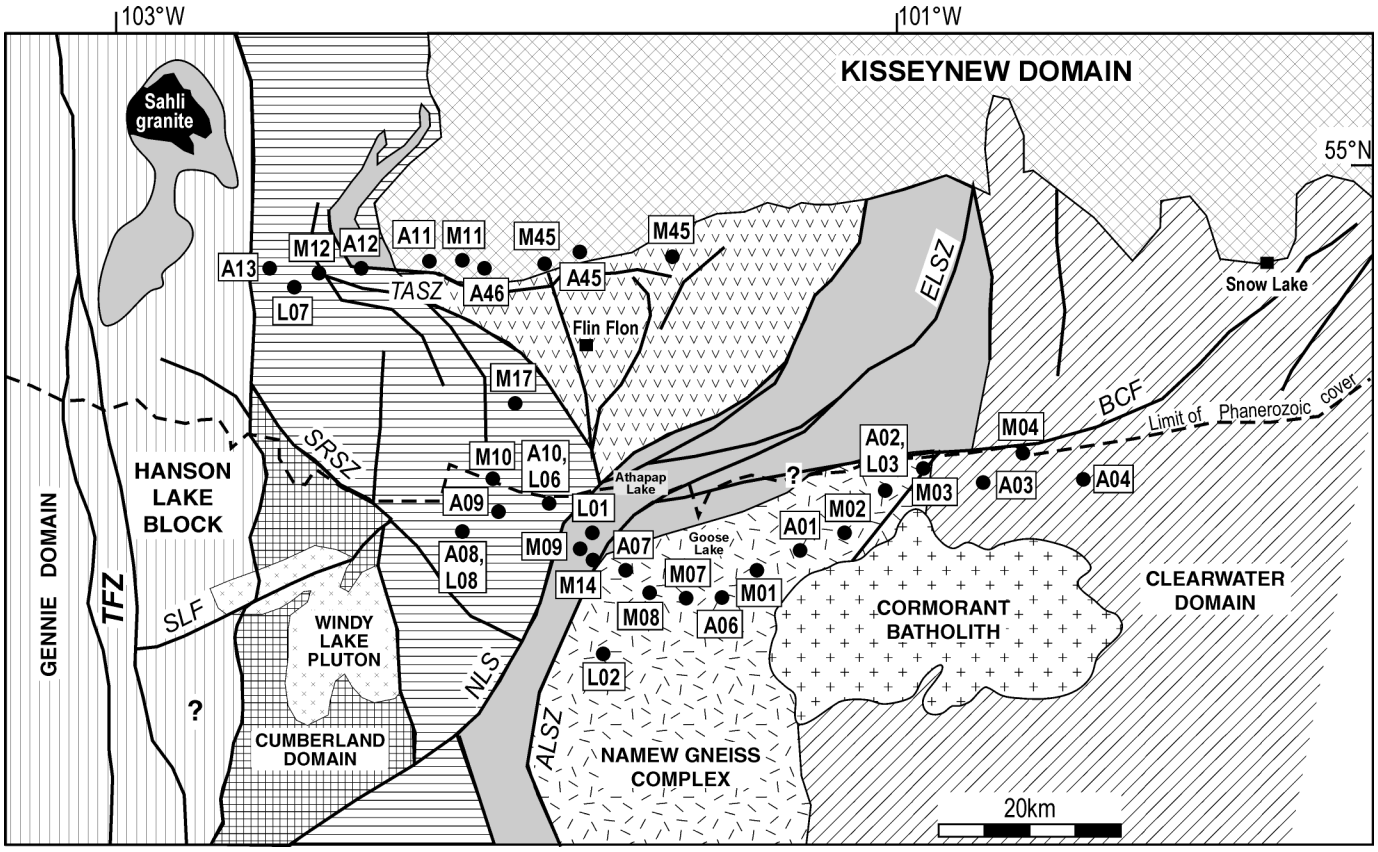

Grant (1997) described preliminary integrated results from across the transect and White et al. (1999) compared seismic and MT images of the Superior boundary zone.

Geology of the Flin Flon Belt

The Flin Flon Belt is a low-grade metavolcanic–plutonic (greenstone) belt (Figs. 1, 2). MT sites in the northern part of the study area are located on the exposed Precambrian Shield: within the Flin Flon Belt and along the margin of the Flin Flon Belt and the Kisseynew gneiss belt. Most of the sites in the southern part of the survey area are located on thin (<100 m) Phanerozoic cover.

The central Flin Flon Belt consists of a collage of intraoceanic assemblages formed in a range of tectonic environments. These 1.92–1.88 Ga assemblages were tectonically juxtaposed into an accretionary complex, the Amisk Collage, at 1.88–1.87 Ga. (Lucas et al. 1996). Subsequent geological development of the region, between 1.88 and 1.69 Ga, was influenced by intracontinental tectonics associated with collision and postcollision of the bounding Archaean cratons. The Amisk Collage was intruded by felsic to mafic intrusive rocks from 1.88 to 1.84 Ga (Lucas et al. 1996). During this same period, sedimentary, volcanic, and volcaniclastic rocks were accumulated in a series of relatively small (successor) basins.

The Amisk Collage suffered pronounced deformation following the end of arc magmatism at ca. 1.84 Ga. Collision of the juvenile terranes of the Reindeer Zone with Archaean cratons, between 1.84 and 1.80 Ga, produced peak metamorphism, penetrative deformation, and southwest thrusting. Within the Amisk Collage, structures created include steeply dipping shear zones, north-trending folds, and associated foliations (Lucas et al. 1996). Terminal collision with the Archaean cratons occurred at 1.83–1.80 Ga, and the central Flin Flon Belt was structurally isolated as a 10–15 km thick imbricate. Postcollisional deformation (after 1.8 Ga) produced a conjugate set of north-northeast- and north-northwest-trending high-angle faults. Late-faulting produced more east-trending faults, e.g., the Athapapuskow Lake shear zone and Berry Creek fault (Lucas et al. 1996).

The Amisk Collage is bounded to the east by the Snow Lake Assemblage, which has undergone a similar deformation history. The Flin Flon Belt is bounded to the north by the Kisseynew gneiss belt, dominated by migmatitic, amphibolite-grade, turbiditic greywackes deposited in a basin adjacent to the Flin Flon arc at ca. 1.85–1.84 Ga (Ansdell et al. 1995; David et al. 1996). Magmatism in the Kisseynew Belt was coeval with south to southwest thrusting of the belt over the Amisk Collage, which occurred as both units overthrust a now largely buried Archaean microcontinent (the Sask Craton, Ashton et al. 1999). The rheological contrast, between the hotter, more ductile Kisseynew Belt and the rela-

tively cold, brittle Flin Flon Domain, led to the formation of east–west-trending structures such as the Tartan – Annabel Lake shear zone at the margin between the two domains.

The Flin Flon Belt is bounded to the west by the Sturgeon-Weir shear zone that separates the belt from the Hanson Lake Block (Maxeiner et al. 1999). The Hanson Lake Block contains volcano-plutonic and intrusive rocks, correlative with the Flin Flon Domain, and Archaean granulite facies rocks of the Sask Craton exposed in a central and a northern window in the block (Ashton and Lewry 1994, 1996; Ashton et al. 1999). Kinematic indicators suggest the Sturgeon-Weir shear zone was formed during the southwest thrusting of the Kisseynew Belt over the Flin Flon Domain (Ashton and Lewry 1994; Ashton et al. 1999).

Leclair et al. (1993, 1997) have interpreted the sub-Palaeozoic geology of the Flin Flon Belt using potential field and drill-core information and extrapolation of units from the exposed shield. In the west of the study area, the Amisk Lake Domain is interpreted to contain mainly low-grade mafic metavolcanic–volcaniclastic rocks and mafic to felsic plutons. To the east of the Amisk Lake Domain, the Athapapuskow Domain consists of a narrow fault-bounded south-trending belt of mafic volcanic and volcaniclastic rocks and related mafic intrusions. Drill core indicates that both mafic and minor felsic rocks exhibit rusty staining due to oxidation of disseminated sulphides. The rocks also contain black, graphitic and sulphitic argillite and minor intercalations of phyllite. The Namew Lake structure is an inferred high-angle fault separating the Amisk Lake and Athapapuskow domains. The Athapapuskow Lake shear zone (ALSZ) separates the Athapapuskow Domain from the Namew gneiss complex to the east, and metamorphic studies indicate that the offset on the ALSZ in the area of Athapapuskow Lake is 10–15 km (Syme 1988; Leclair et al. 1997). Pressure–temperature studies suggest that the rocks to the northwest of the fault formed under pressures of <0.3 GPa, whereas the gneisses to the southeast formed at pressures of 0.5–0.9 GPa (Leclair et al. 1997).

The Namew gneiss complex comprises mainly high-grade orthogneissic rocks and multiple felsic and intermediate intrusives. Leclair et al. (1993) suggest that the complex may have been built up by multiple intrusions of tonalite–diorite sheets at mid-crustal level. Initial ϵ_{Nd} values for Namew plutonic rocks are similar to those obtained for the 1.87–1.84 Ga plutons in the Flin Flon Collage, suggesting that the gneiss complex forms an integral part of the Flin Flon Collage. Exhumation of the gneiss complex occurred after peak metamorphism during faulting associated with postcollisional transpression of the THO (Leclair et al. 1997). The Namew gneiss complex contains a subunit of subordinate supracrustal rocks, composed mainly of amphibolite facies, mafic, psammitic, and pelitic gneisses and occurring mostly as thin (<3 km), elongated units. Both the psammitic and pelitic gneisses are graphite bearing. The supracrustal rocks are interpreted to be metamorphosed and deformed equivalents of Amisk Group rocks (Leclair et al. 1993).

The Namew Lake nickel–copper mine is located within the gneiss complex to the south of the study area. The pipe-like massive sulphide orebody is hosted by a pyroxenite sill enclosed within orthogneisses (Cumming and Krstic 1991*a*, 1991*b*; Menard et al. 1996). Geological studies of the pyroxenite and surrounding gneisses reveal five distinct phases of deformation. The earliest event coincided with metamorphic conditions of 650–700°C (Menard et al. 1996). The rocks underwent upper amphibolite facies metamorphism at 1880–1860 Ma (M_1), lower amphibolite facies metamorphism at ~1830 Ma (M_3,), and greenschist facies metamorphism at 1740–1720 Ma (M_5).

The Cormorant Batholith is a large (60 × 25 km), dominantly monzogranite intrusion in the southeast of the study area. It has been dated at 1830 Ma using zircon U–Pb ages from several cores (Leclair et al. 1997). The Clearwater Domain is a broad south- to southwest- trending volcano-sedimentary belt, which is tentatively interpreted to be equivalent to the Snow Lake Assemblage. There is a progressive decrease in metamorphic grade from the margin of the Namew gneiss complex towards the east in the Clearwater Domain, suggesting the Namew Gneiss and the Clearwater Domain form an oblique crustal section.

Geophysics of the Flin Flon Belt

Seismic reflection

Lithoprobe seismic reflection profiles have been interpreted to show that the internal zone of the THO has been subjected to thick-skinned style deformation with significant dipping reflective zones extending from the surface to Moho depths (Lucas et al. 1994; White et al. 1994). Figure 3 shows the seismic reflection profiles from the study area.

The Amisk Collage and Snow Lake Assemblage (Domain B in Fig. 3) are dominated by diffractions and diffuse, incoherent reflections. This response is attributed to low bulk deformation state, heterogeneous distribution of deformation zones, and steep dips (White et al. 1994). The Namew gneiss complex (Domain C) is characterized by laterally continuous reflective zones separated by less reflective zones. The moderately reflective units form a 50 km wide band of rocks dipping 20° to the east. The domain contains a series of arcuate reflectors that sole into the east-dipping planar reflections. These reflections could represent layer-parallel, relatively transparent, plutonic sheets separated by reflective screens of highly deformed country rock (White et al. 1994). The gneiss complex overlies a zone of strong east-dipping reflectivity (Domain A) that is approximately 20 km thick and is interpreted to be a package of lower crustal rocks of the same tectonic affinity as the Namew gneiss complex. The Flin Flon Belt and the Namew Gneiss are in near-vertical contact at the ALSZ (White et al. 1994). This structure appears in the seismic sections as a narrow, near-vertical, transparent band visible to a depth of at least 6 s two-way traveltime (TWT), or approximately 18 km.

Lucas et al. (1994) provided an interpretation of the seismic reflection profiles crossing the northern margin of the Flin Flon Belt. The low-reflectivity rocks of the Flin Flon Belt (Domain B) are segmented into a series of blocks separated by late orogenic high-angle faults (Fig. 3) that all appear to terminate at, or above, a mid-crustal detachment fault. The footwall of the detachment comprises highly reflective rocks (Domain A), interpreted to be mid- to low-crustal arc-derived gneisses. Towards its northern margin, the Flin Flon Belt is floored by a second detachment sepa-

Fig. 3. Seismic reflection response of the Flin Flon Belt (from Lucas et al. 1994). (*a*) West–east profile for seismic reflection lines 9, 5, and 3. (*b*) South–north profile for seismic reflection lines 7*a*–7*c*.

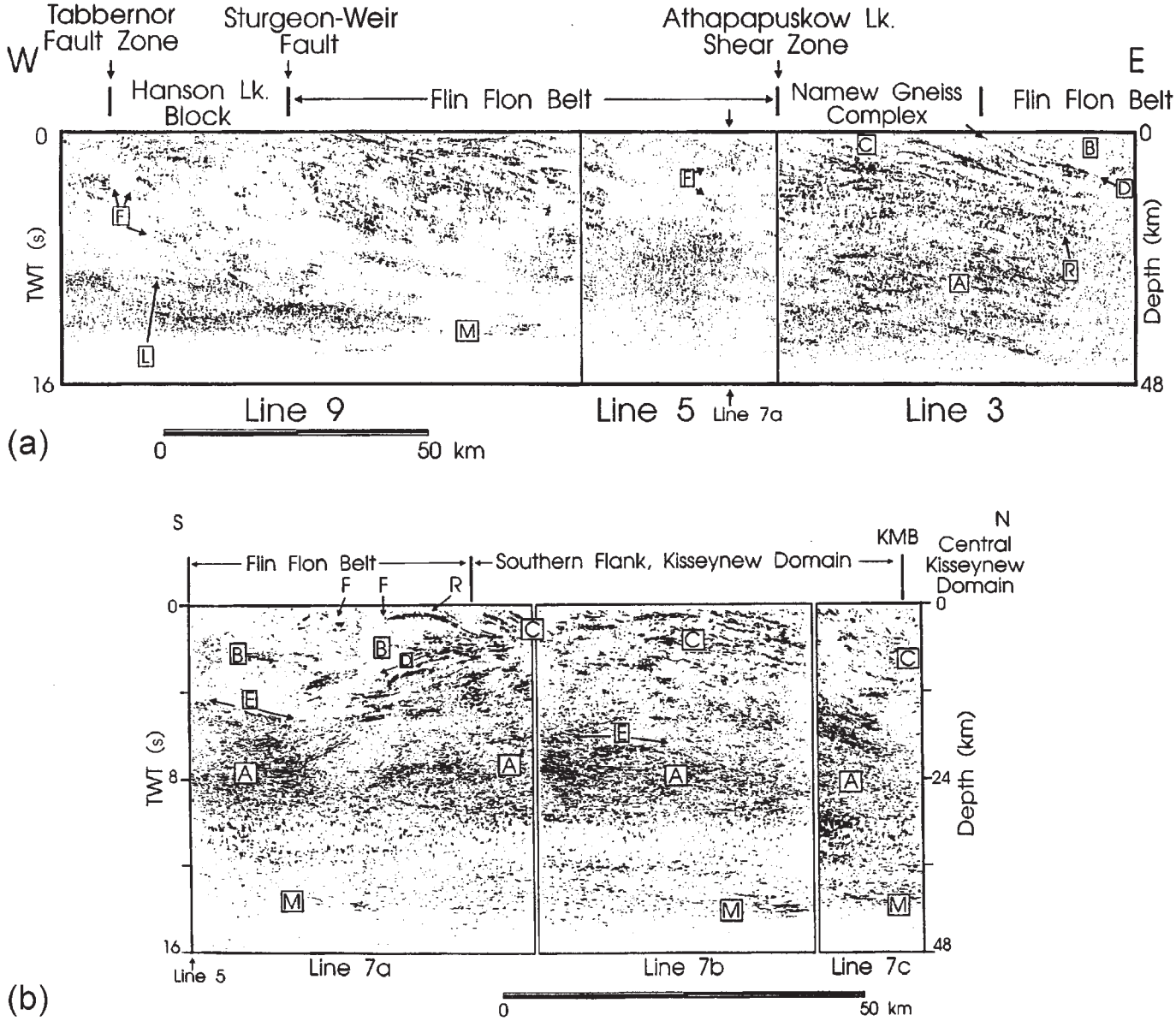

rating it from moderately reflective rocks interpreted as correlating with the Namew gneiss complex. At the surface, the Flin Flon Belt is overlain by the southern flank of the Kisseynew Belt. The boundary is interpreted as a series of thrust faults or highly strained ductile fold nappes.

Potential field and airborne electromagnetic anomalies

One of the strongest magnetic features observed in the sub-Palaeozoic Flin Flon Belt is a 10–12 km wide linear belt associated with the Athapapuskow Domain. The magnetic response within this zone is attributed to volcanic rocks, and the high magnetic gradient at the south of this zone is attributed to an iron formation (Hosain 1984). The Namew gneiss complex is characterized by a more neutral aeromagnetic signature containing curvilinear cusp-shaped highs associated with the subordinate supracrustal rocks found in the complex (Leclair et al. 1993, 1997). These magnetic highs are commonly associated with strong airborne EM conductors, and a number of holes drilled by mining companies in these zones have intersected barren massive sulphides (Hosain 1984). In the vicinity of the Namew Lake mine, two distinctive conductive horizons that appear across a 20 × 30 km area are associated with a graphite-bearing pyrite and pyrrhotite-rich greywacke volcaniclastic unit and a pyrite and pyrrhotite-rich horizon in mafic volcanic rocks (Menard et al. 1996). Compilation maps show numerous east–west-striking airborne EM anomalies in Goose Lake, just to the northeast of the MT profile (Truman 1992).

Magnetotelluric methodology

Basic principles

The MT method is based on simultaneous measurements of the two orthogonal horizontal components of the time-

varying electric (***E***) and magnetic (***H***) fields (e.g., Vozoff 1991). In high-frequency (short period) surveys, called audio-frequency MT, or AMT, atmospheric sources (distant lightning) provide the natural signals, whereas for low-frequency (long period) surveys, the signals are induced by magnetospheric and ionospheric sources. As a consequence of the skin-depth phenomenon in electromagnetism, depth information is obtained in MT surveys by analysis of the response as a function of increasing period. Short-period MT signals (10^{-4}–10^{-3} s) typically penetrate 0.5–10 km into the upper crust, whereas long-period signals (10^{3}–10^{4} s) typically penetrate 100 km or greater into the upper mantle.

MT analysis usually commences with calculation of the MT impedance, the frequency-domain ratio of orthogonal horizontal electric and magnetic field components:

$$Z_{ij}(\omega) = \frac{E_i(\omega)}{H_j(\omega)}$$

In general, the electric and magnetic fields are measured in both horizontal directions (i,j) allowing definition of four components of the impedance:

$$\mathbf{Z}(\omega) = \begin{bmatrix} Z_{ii}(\omega) & Z_{ij}(\omega) \\ Z_{ji}(\omega) & Z_{jj}(\omega) \end{bmatrix}$$

For a one-dimensional (1D) horizontally layered conductivity structure, the diagonal impedance matrix terms are zero, $Z_{ii}(\omega) = Z_{jj}(\omega) = 0$, and off-diagonal terms differ only in sign $Z_{ij}(\omega) = -Z_{ji}(\omega)$. For a two-dimensional (2D) structure, in which conductivity is invariant in one horizontal direction, the diagonal terms will be zero if the EM fields are defined in a coordinate system orthogonal to the strike of the structure. In this case the impedance component for the electric field parallel to strike, called the *transverse electric (TE)* mode, will differ from the component with the electric field perpendicular to strike, the *transverse magnetic (TM)* mode. If the impedance is measured in an arbitrary orientation, the angle required to rotate the measurements into TE and TM modes can be determined from the impedance tensor. The impedance data can thus be used to determine the geoelectric strike of a conductivity structure that responds in a 2D manner at the periods of interest. For a three-dimensional (3D) conductivity structure, the impedance will have a more complex form but is often presented after rotation to the best-fitting 2D form.

Different averaged responses are commonly used to represent the impedance response for 2D and 3D MT data. These averages combine two or four impedance components to provide a response that can be interpreted using 1D methods. The resulting conductivity structure will be an approximation to the true structure. In our analyses we use the determinant response, defined by

$$Z_{\mathrm{det}}(\omega) = \sqrt{Z_{ij}(\omega)Z_{ji}(\omega) - Z_{ii}(\omega)Z_{jj}(\omega)}$$

Magnetotelluric response

The magnitude of the MT impedance is commonly expressed in terms of the apparent resistivity $\rho_a(\omega)$ using the relationship

$$\rho_a(\omega) = \frac{1}{\omega\mu}\left|Z_{ij}(\omega)\right|^2$$

Apparent resistivity is a weighted-average resistivity over the penetration depth of the signals. It equals the resistivity of the uniform half-space possessing the same response as the observed datum. The MT response is almost always specified in terms of the apparent resistivity and the impedance phase.

The impedance phase, the phase lead of the measured electric field over the measured magnetic field, provides important information on the conductivity structure additional to what can be obtained from the apparent resistivities (see, e.g., Cavaliere and Jones 1984). For MT measurements made over a uniform half-space the Z_{xy} phase will equal 45° and the Z_{yx} phase will equal –135° (due to the right-hand rule). For 1D and 2D structures, the Z_{xy} phase lies between 0 and 90° (–180 to –90° for Z_{yx}) and for most 3D structures it is observed also to fall within this range. The phase response at a particular period will provide an indication of the vertical gradient of conductivity at the penetration depth corresponding of the signals. Phase values exceeding 45° (or –135°) indicate that the conductivity is increasing with depth, whereas phase values less than 45° indicate the conductivity is decreasing with depth.

For 2D structures the phase will be different between the TE and TM modes. This difference allows the phase response to be analyzed for geoelectric strike. For data measured in an arbitrary coordinate system over a 2D structure, the phase of the off-diagonal impedance terms will be a weighted average of the TE and TM phase. If such data are progressively rotated through a range of coordinate-system orientations, then the angle at which the difference between phase terms is greatest will correspond to the orientation of the conductivity structure (to within a 90° ambiguity, which may often be resolved by considering the magnitude of the two phase values).

Two-dimensional MT apparent resistivity and phase response are often presented in the form of pseudosections. These diagrams contour the value of apparent resistivity or phase as a function of distance (site location) along the abscissa (horizontal axis), and log (period), as a proxy for depth, increasing down the ordinate (vertical axis). Apparent resistivity is often contoured using logarithmically spaced contour intervals, as the parameter varies over many orders of magnitude. The depth of penetration of MT signals increases with increasing period, so an apparent resistivity pseudosection will correspond to a smoothed form of the true resistivity – depth section.

Galvanic distortion of the magnetotelluric response

Electric charge accumulation on near-surface (local) heterogeneities can distort the measured MT response so that it no longer accurately represents the larger scale (regional) conductivity structure. If the dimensions of the heterogeneity are much smaller than the signal penetration into the surrounding rocks, the distortion will affect mainly the electric fields, and will be independent of frequency. In its simplest form, that is, when the acquisition coordinate system and the regional strike direction are the same, the galvanic distortion affects the two horizontal electric field

components independently, causing a scaling of the impedance magnitude and thus apparent resistivity response. This distortion is called static shift (Jones 1988), and a number of techniques have been proposed to deal with it. The phase response retains its correct form and can be used to derive the conductivity structure, but only with relative conductivities, not absolute ones. In the typical case of the acquisition and interpretation coordinate systems not being aligned, galvanic charges cause a mixing of the impedance tensor terms, a situation commonly referred to as MT tensor distortion. The distortion of an MT response by local structures reduces the resolution of the deeper structure, but at the same time provides a measure of the density of localized conductivity features at shallow depth.

A widely adopted MT tensor decomposition method is that of Groom and Bailey (1989, 1991; Groom et al. 1993). This method involves fitting observed MT data with a model that is based on a galvanic electric field distortion of a 1D or 2D regional MT response. The phase-related galvanic distortion at each frequency is characterized by two parameters: *shear*, which provides a measure of the local polarization of the electric field response, and *twist*, which provides a measure of its local rotation. Shear and twist are usually described as angles by taking their tangents. These two distort the phases, whereas the apparent resistivities are distorted by these two plus the static shifts that cannot be determined from the MT responses themselves. The remaining shift effects are defined by Groom and Bailey as local *anisotropy*, which splits the two apparent resistivity curves apart by magnifying the amplitude of the electric field in one direction and reducing it in the perpendicular one, and local *site gain*, which shifts both curves by the same amount. Theoretical studies have shown that whereas anisotropy can be large, site gain is typically very small and shifts the apparent resistivity curves less than 20% (Groom and Bailey 1989).

The shear angle defined in the Groom–Bailey decomposition provides a useful measure of the degree of distortion. Shear angles close to zero (<10°) indicate minimal polarization (<20%) of the local electric field and very low distortion, whereas angles in the range 10–30° indicate moderate levels of polarization (20–60%), and thus moderate distortion. For sites with low to moderate distortion, it is usually possible to recover good estimates of the regional TE and TM responses. Shear angles of 30–45° characterize strong distortion (60–100%) and at sites with this level of shear it is commonly difficult to recover the two regional impedance values. This is because the electric field is very strongly polarized, so information can only be obtained in the polarization direction, which may not be either the TE or TM mode.

Induction vector response

The induction vector is a graphical representation of the transfer function between the horizontal magnetic field components and the vertical magnetic field component created by electric currents induced in the Earth. Over a uniform 1D Earth, there are no vertical magnetic fields, so these vectors have zero length. Vectors are plotted to point towards conductors or more conductive parts of the Earth. The lengths of the vectors are proportional to the conductivity contrast but also decrease with distance from the conductor. Since the penetration of EM signals increases with increasing signal period, longer period induction vectors will correspond to a deeper and larger spatial scale response.

Lithoprobe MT survey and data processing

Survey configuration

Data acquisition for the Lithoprobe THOT reconnaissance MT survey was undertaken between June and September 1992 by a commercial contractor (Phoenix Geophysics). The survey involved data collection at two types of recording sites: audio-frequency only MT (AMT-only) sites, which provided the MT responses for the audio-frequency period range of 10^{-4}–10^{-1} s, and broadband AMT–MT sites, which provided the AMT and MT responses for the period range 10^{-4} to almost 2000 s. Data were acquired at a total of 56 AMT–MT sites and 52 AMT-only sites located along an 800 km long profile across the THO following seismic reflection lines 3 and 9 (Fig. 1). The survey configuration provided an average spacing between MT data acquisition locations of about 15 km, and an average spacing between AMT data acquisition locations of about 7 km.

The AMT responses at each site were based on at least 6 h of recording, usually acquired between 10:00 and 16:00 (local time), and the MT responses were derived from a minimum of 24 h of recording (typically 40 h). Electric field recordings were made using orthogonal E-lines of 100 m or greater, and horizontal magnetic field recordings were made using induction coil sensors, with different coils for AMT and MT. Vertical magnetic field recordings were made using a coil for AMT, and a multi-turn square 10 × 10 m loop for MT. Remote-reference magnetic field recordings were made using induction coils at a distance of least 100 m from the main site for AMT, and at least 1 km for MT. Utilizing these remote-reference data avoids biases in the response estimates due to noise on the local magnetic field recordings (Gamble et al. 1979).

The long-period MT survey was completed by personnel from the University of Manitoba as a follow-up survey to the reconnaissance MT survey. The MT recordings were made using Long-period Magnetometer System (LiMS) instruments, designed and manufactured by the Geological Survey of Canada, during August 1992. The instruments were configured for the survey with three-component fluxgate magnetometer sensors and orthogonal E-lines of length 60–100 m. Recordings were overlapped in time at adjacent sites in order to provide remote-reference time series (involving sites typically 20–40 km apart). The total recording time at each site was 6–12 days, providing the MT response for the period range 40–10^4 s.

In total, MT recordings were made at 14 broadband AMT–MT sites (Mxx), 14 AMT-only sites (Axx), and six long-period sites (Lxx) in the Flin Flon Belt and arc-related geological units to the north and south of the belt (Table 1; Fig. 2).

Data processing

Phoenix Geophysics provided the MT responses for each site in the form of auto- and cross-power spectra of the seven EM components. The spectra were computed using robust statistical techniques based on the Jones–Jödicke ap-

Table 1. Location of MT sites in the Flin Flon Belt and adjacent areas.

Broadband MT sites			AMT sites			Long-period MT sites		
	Lat. N	Long. W		Lat. N	Long. W		Lat. N	Long. W
M01	54°26′20′′	101°21′10′′	A01	54°27′50′′	101°14′45′′	L01	54°28′40′′	101°47′30′′
M02	54°29′00′′	101°09′15′′	A02	54°32′45′′	101°02′15′′	L02	54°19′40′′	101°45′00′′
M03	54°34′30′′	100°56′30′′	A03	54°34′00′′	100°47′30′′	L03	54°33′00′′	101°01′40′′
M04	54°35′25′′	100°41′10′′	A04	54°34′10′′	100°32′00′′	L06	54°31′25′′	101°52′55′′
M07	54°23′40′′	101°32′45′′	A06	45°24′00′′	101°26′40′′	L07	54°49′30′′	102°33′50′′
M08	54°23′40′′	101°38′25′′	A07	54°26′30′′	101°42′20′′	L08	54°28′43′′	102°06′29′′
M09	54°27′20′′	101°48′55′′	A08	54°28′50′′	102°06′20′′			
M10	54°33′35′′	102°02′10′′	A09	54°31′05′′	102°00′40′′			
M11	54°51′45′′	102°07′20′′	A10	54°31′25′′	101°52′55′′			
M12	54°50′35′′	102°29′00′′	A11	54°52′10′′	102°12′25′′			
M14	54°27′05′′	101°45′50′′	A12	54°51′35′′	102°21′35			
M17	54°39′50′′	101°58′50′′	A13	54°50′40′′	102°36′45′′			
M45	54°50′46′′	101°54′41′′	A45	54°52′33′′	101°49′07′′			
M46	54°51′53′′	101°34′49′′	A46	54°50′47′′	102°02′57′′			

proach (Jones and Jödicke 1984; method 6 in Jones et al. 1989). Time series collected in the long-period MT survey were analyzed using the same robust processing procedures but with jack-knife error estimation.

Detailed examination of the responses subsequent to the survey revealed band-limited noise in the MT data from several sites with relatively narrow band spectral peaks centred on 700 Hz. The noise is characterized by a strong peak in the vertical magnetic field spectra and is present in one or both horizontal magnetic field spectra and one or both horizontal electric field spectra. The proximity of the affected sites to railways and mining camps indicates that the noise is related to industrial activity. Because of the noise, the short-period responses at contaminated sites (A11, M11, A46, M45, M17, M01, and A01) were excluded from further analysis.

Magnetotelluric response in the Flin Flon Belt

Overview from determinant impedance response

Figure 4 shows the determinant apparent resistivity and phase pseudosections for the two east–west profiles crossing the north and south parts of the Flin Flon Belt. The responses show some local variation between the apparent resistivities at adjacent sites, which can be attributed to galvanic distortion of the response. However, the data do exhibit systematic responses between multiple sites. At many sites the response approximates that of a three-layer structure: apparent resistivities are relatively low at short periods, high at intermediate periods, and decrease at long periods. Low phase values at short periods reflect the increasing resistivity with depth in the upper crust, whereas high phase values at intermediate to long periods indicate the transition to more conductive deep crustal rocks.

A prominent feature in the MT response is the difference between the north and south regions of the Flin Flon Belt. On the northern profile, the intermediate-period response (10^{-2}–10^{2} s), corresponding to signal penetration into the upper and mid crust, infers that the rocks at those depths are much more conductive than over most of the southern profile. The effect manifests itself as both lower apparent resistivity and higher phase values on the northern profile.

A second significant feature visible in Fig. 4 is the effect due to a conductor at sites near Athapapuskow Lake. The response is relatively conductive at periods $>10^{-2}$ s at sites extending from M09 to M07. At site M14, the apparent resistivity decreases to a value of <1 Ω·m at a period of ~10^{2} s. This crustal conductor revealed by the MT response is named the Athapapuskow Lake conductivity anomaly (ALCA). There is no corresponding conductor observed on the northern profile. However, because of both the larger MT site spacing employed in this area and data limitations caused by industrial noise, it is possible that a similar-sized conductive feature to the north or northeast in the Flin Flon Belt has been missed by the Lithoprobe survey.

Sites in the central and eastern parts of the south profile were located on thin Phanerozoic cover. It is evident from Fig. 4 that the effect of the Phanerozoic cover on the MT response was minimal. There is no significant decrease in the short-period apparent resistivity at these sites.

Galvanic distortion and tensor decomposition

The galvanic distortion in the Flin Flon Belt was examined using Groom–Bailey decomposition. In particular, the shear at each site was studied as a function of period in three relatively broad period bands (10^{-4}–0.015, 0.02–4, and 5–950 s), to provide stable estimates spanning the available data. Figure 5 shows the results of this analysis in histogram form. It provides an overview of galvanic distortion levels in a Proterozoic greenstone belt where the galvanic distortion level is strong, with many sites having shear values exceeding 30° in the longest period band. Analyses using narrower period bands revealed that at periods >100 s the shear value at most sites exceeds 35°.

These distortion results demonstrate that the MT response at periods ≤100 s can be used to define the upper- and mid-crustal structure of the Flin Flon Belt. However, the high levels of distortion at long periods means that the data are not suitable for investigating the conductivity structure of the lower crust and mantle lithosphere without significant care. The MT data can provide only poor resolution of 2D struc-

Fig. 4. Determinant apparent resistivity and phase sections for east–west profiles across the Flin Flon Belt. The circles show the data used in the contouring. The upper two panels are for a northern profile including sites A13 to M46. The lower two panels are for a southern profile including sites M10 to A04. Contour intervals are the same for both profiles.

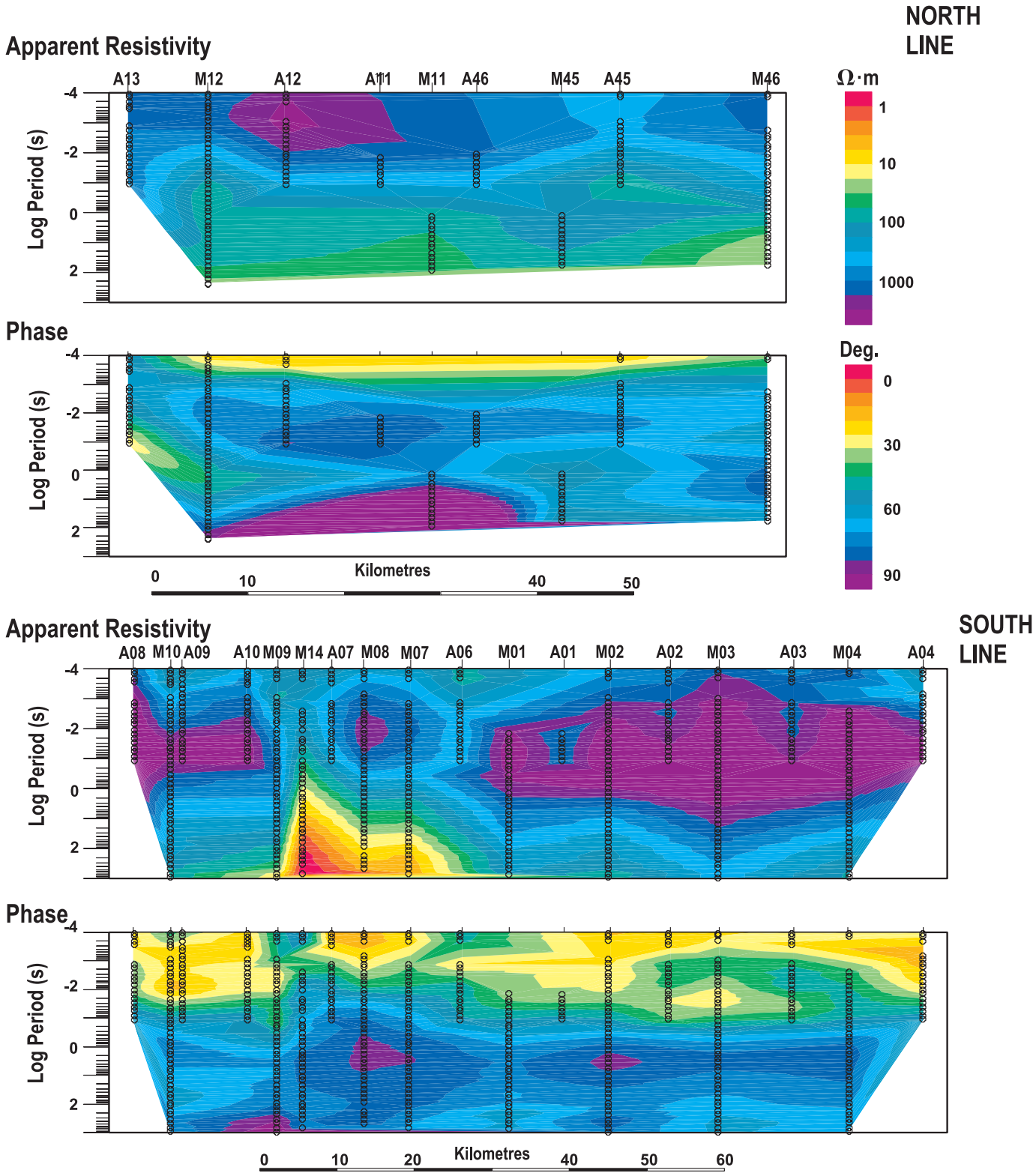

Fig. 5. Distribution of shear at sites in the Flin Flon Belt. Galvanic distortion at sites in the Flin Flon Belt as characterized in terms of the absolute value of the shear angle. Results are for three period ranges: band 1, 10^{-4}–0.015 s; band 2, 0.02–4 s; and band 3, 5–950 s; and the shear values have been grouped into 10° bins.

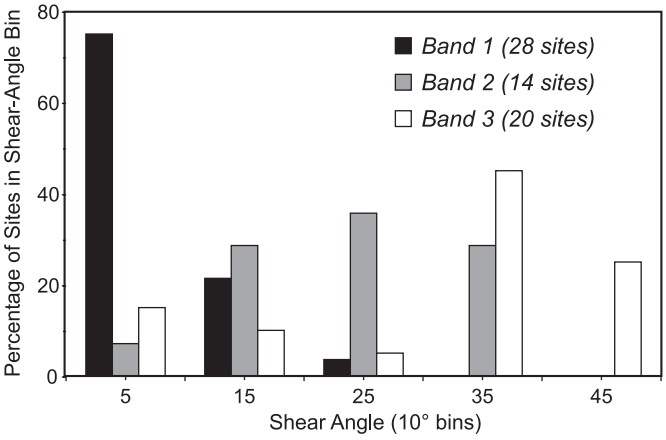

ture at these depths. The average shear for the six LiMS sites in the belt (period range 40–4000 s) is 35°, and at site L08 the electric field is completely polarized (shear 45°). For the rest of this study, we will use only the induction vector response from these sites.

Figure 5 shows that the level of galvanic distortion increases progressively with increasing period. The shear is typically <10° at periods less than 10^{-2} s, between 20–30° at periods around 1 s, and >30° at periods exceeding 10 s. This pattern is observed for most individual sites as well as for the ensemble grouping in Fig. 5. The pattern differs from the "classical" Groom–Bailey physical model in which a near-surface structure produces a frequency-independent shear and twist of the electric field. This indicates that the distorting 3D structures in the Flin Flon Belt are distributed over a wide depth range in the crust. The complex surface geology (Fig. 2) and seismic response (Fig. 3) in the area both suggest that it is reasonable to expect numerous small-scale resistivity structures, associated with faults and lithological changes, throughout the upper and mid crust.

To complete the MT analysis in the Flin Flon Belt, it is necessary to perform full tensor decomposition of the MT tensor to obtain the best estimates of the regional 2D MT responses in the most appropriate strike direction. As the galvanic distortions at most sites do not conform to the assumed Groom–Bailey model over the whole period range, we concentrate on fitting the model to the period range 10^{-3}–10^{2} s, most appropriate for examination of upper- to mid-crustal structures. The decomposition at each site proceeded through unconstrained Groom–Bailey inversion, followed by iterative determination and constraint of the average shear, twist, and regional strike. In the subsequent step, the average regional strike was estimated for groups of sites with a spatially consistent response, and a final Groom–Bailey decomposition performed with the regional strike set to this value.

Groom–Bailey tensor decomposition is based on the approximation that the regional geoelectric structure is either one- or two-dimensional. At most sites in the Flin Flon Belt the Groom–Bailey model for the impedance reproduces most features of the observed impedance but there are minor differences between the model and observed response, particularly in smaller magnitude impedance components and at higher frequencies. This misfit is not surprising considering the strong galvanic distortion in the belt and the complex near-surface geological structure. Considering all sites in the study area, the Groom–Bailey model provides a reasonable representation of the regional MT response. Further tensor decomposition analysis may provide some fine tuning of the regional MT response at several sites. Jones and Grant (1997) have performed multisite, multifrequency decompositions for these sites using the method of McNeice and Jones (1996). We use the results of that study here to help define the overall regional strike. It is also possible that it will be necessary to consider galvanic distortion of both the electric and magnetic fields (e.g., Zhang et al. 1993; Chave and Smith 1994) to define fully the distortion at some of the sites in the study area.

Large-scale geoelectric structure in the Flin Flon Belt

Geoelectric strike directions

A primary aim of the THOT Lithoprobe MT survey was to provide a reconnaissance of the major geoelectric structures crossed in the transect (Clowes 1993). The geoelectric strike direction is a useful parameter for defining the different geoelectric structures detected by the MT data. Here we use three measures to define regional geoelectric strike:

(1) Induction vectors: The direction of the reversed real component of the induction vector will be orthogonal to the local geoelectric strike and will point towards more-conductive regions. For 2D structures, the imaginary component of the induction vector should be parallel or antiparallel to the real component, and departures from such a situation reveals the extent of 3D structures. Induction vectors can be used to resolve the inherent ±90° ambiguity in the Groom–Bailey regional strike and the strike estimated from the maximum phase-split orientation.

(2) Maximum phase-split orientations: This parameter has a ±90° ambiguity when used as a strike estimate, but we can examine the data in a consistent manner using the direction of the larger phase. For locations in which there are isolated conductors in resistive background rocks the larger-phase direction will usually (but not always) correspond to the geoelectric strike. The maximum phase-split rotation is relatively robust (±15°) in the presence of moderate distortion (shear, twist <20°).

(3) Groom–Bailey regional-strike: Because of the number of parameters fitted in Groom–Bailey decomposition, stable estimates of the regional strike require its estimation over relatively broad period bands. To obtain stable regional strikes for the strongly distorted sites in the Flin Flon Belt it was necessary to use period band of at least 3 decades in width. Because of the ±90° ambiguity in this strike estimate, we examine the data with all strikes adjusted to be in the quadrant centred on N35°E.

Figure 6 shows geoelectric strike indicated by these three parameters for short (0.01 s), intermediate (5 s), and long (50 s) periods. The short periods correspond to signal penetration into the upper crust and the long periods to signal

Fig. 6. Geoelectric strike in the Flin Flon Belt as a function of period. The induction vector plot shows the real reversed component (darker arrow with head and error ellipse) and the imaginary component (light arrow without head). The maximum phase-split orientation is plotted in the maximum-phase direction with the length of each vector proportional to the phase split. The longest vectors represent a 90° split. The Groom–Bailey regional strikes are shown for three period bands: band 1, 10^{-3}–10^{-1} s; band 2, 10^{-2}–10 s; and band 3, 1–1000 s. Vectors have been adjusted to lie in the quadrant around N35°E, and their length indicates the goodness of fit of the Groom–Bailey model. The location of the Athapapuskow Lake conductivity anomaly (ALCA) is traced on the induction vector plots. The western edge (dashed line) is coincident with the Athapapuskow shear zone. The eastern edge is less well defined, and its approximate location is shown by the dotted line.

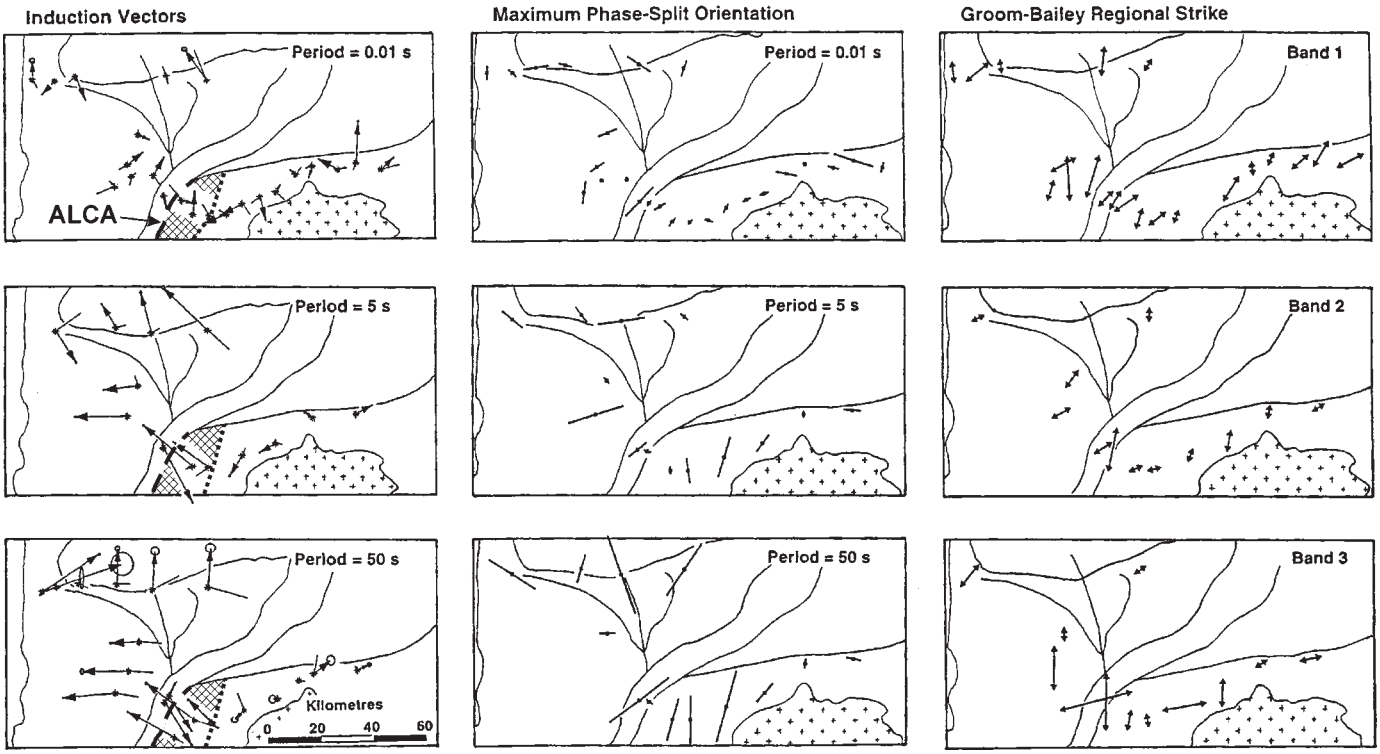

penetration into the deeper parts of the mid crust. The MT results provide the first-order recognition of four large-scale geoelectric "regions" in the Flin Flon Belt, which may be considered as the geoelectrical analogue of areas of uniform reflectivity recognized in a seismic reflection section.

Athapapuskow Lake area

The first group of sites is centred on the area of the ALSZ and Namew Lake structure. At short periods (≤0.01 s), induction vectors are small (<0.3) and exhibit inconsistent orientation between adjacent sites, indicating that the response is dominated by local conductivity structures. At long periods, the response becomes more uniform and the real induction vectors point in a northwest or southeast direction. Maximum phase-split directions have a relatively consistent northeast alignment across the Athapapuskow Lake area. The Groom–Bailey regional strike is more variable as a function of both position and period but the general trend is in a northeast direction (Fig. 6). Jones and Grant (1997) performed a multifrequency, multisite analysis of MT sites extending from M09 to M02 and found dominant Groom–Bailey strike angles of N57°E for the period range 10^{-2}–1 s and N0°E for the range 10–1000 s. The overall results suggest the shallow structure (sensed at periods of $<10^{-2}$ s) is east-northeast–northeast striking and the deeper structure (sensed at periods ≥10 s) includes a north-northeast–northeast-striking linear conductor located in the vicinity of the ALSZ or Namew Lake structure.

The conductor defined by the geoelectric strikes corresponds to the ALCA recognized in the determinant impedance responses (Fig. 4). It is the best resolved of the structures in the Flin Flon Belt and its modelling and detailed geological interpretation are discussed below.

The relatively large (average 7 km) site spacing of the reconnaissance MT survey, combined with the complex geology of the Flin Flon Belt, permits only a qualitative interpretation of the remaining major geoelectric responses recognized in the belt. A more significant constraint is that the geoelectric strike of these structures is parallel, or at low angle, to the survey profile and it is therefore impossible to constrain properly 2D models. We therefore restrict interpretation to a tentative association of each geoelectric response with its probable geological source.

Sites near the Cormorant Batholith

A group of sites in the east of the study area exhibit a relatively systematic response. The induction vector at these sites is quite small and less spatially consistent than for the other groups of sites, but there is an overall tendency for real vectors at the western sites to point to west– southwest, and for real vectors at eastern sites tend to point east. The short- and intermediate-period Groom–Bailey regional strikes tend

to be oriented northeast–north-northeast, whereas the longer-period strikes are more consistently north–south or east–west. The maximum phase-split orientations for these sites rotate from southwest–northeast at the western edge of the group (M01, M02) around to east–west or east-southeast in the east (M03, M04). The responses observed for this group of sites are consistent with small-scale structures that strike north-northeast and with the presence of a large resistive body to the south of the sites.

The resistive body is clearly the Cormorant Batholith (Fig. 2). The sites in this area are located in the Namew gneiss complex and Clearwater Domain, but all lie within 10–20 km of the batholith. The maximum phase-split orientations at 10^{-2} s period define an arcuate shape parallel to the margin of the batholith, and real induction vectors point away from it. These results show that the dominantly monzogranitic batholith is considerably more resistive than the surrounding gneissic rocks, and that it produces a strong influence on the regional geoelectric response. The MT responses are unlikely to be able to provide any more information on the structure of the batholith than is available from potential field data.

Amisk Lake area

Three sites in the southwest of the study area (A08/L08, M10, and M17), located to the east of Amisk Lake, have a spatially consistent geoelectric response. Real induction vectors point west at periods ≥5 s, and imaginary vectors point in an antiparallel direction at periods ≥50 s (Fig. 6). Groom–Bailey regional strikes are aligned northeast–east-northeast at intermediate periods, but swing to a north direction at long periods. Maximum phase-split directions are generally northeast–east-northeast at periods <5 s, while the one resolved direction at 50 s has an east orientation. Taken together, the three responses from this group of sites suggest a north–north-northeast geoelectric strike. The magnitudes and phase values of the impedance tensor elements are consistent with the sites being located to the west, and on the more conductive side, of a resistivity boundary.

Examination of the locations of the sites on detailed geological maps (e.g., Fig. 2, Lucas et al. 1996) suggests that the resistivity contrast detected at those sites is also a contrast between resistive intrusive rocks and more conductive gneisses. The geoelectric response is probably associated with the east-to-west transition from resistive, felsic, arc intrusives, including the Reynard Lake, Kaminis Lake, and Boot–Phantom plutons, to the ocean-floor, ocean-plateau, and arc volcanic rocks of the Birch, Sandy Bay, and West Amisk assemblages.

Northern margin of Flin Flon Belt

The final group of sites with spatially consistent geoelectric response consists of the sites located near the margin of the Flin Flon Domain with the Kisseynew Belt. At periods ≤5 s, real induction vectors are aligned west-northwest or east-southeast, suggesting a conductor running parallel to the geological boundary. At longer periods the real vectors at eastern sites have a north orientation, whereas vectors at western sites have a northeast orientation. At these periods the imaginary vectors are not aligned with the real vectors, suggesting a complex geoelectric structure. The maximum phase-split orientations at 10^{-2} s are mostly close to north–south or east–west, and become more variable at longer periods. The regional strike is poorly defined in this area because of the removal of data affected by industrial noise, but results from M12 and M46 suggest a northeast strike.

The combined responses indicate that the shallow geoelectric strike is roughly east–west but varies locally. The east–west-oriented shallow geoelectric structure is subparallel to the strike of the geological units and the Tartan–Annabel shear zone (Fedorowich et al. 1995) (Fig. 2). There is insufficient site density to identify specific conductive units or structures.

The divergence of the real and imaginary induction vector directions and the irregularity of the impedance strike and maximum phase split suggest that the deeper structure is 3D in form. This complex geoelectric response is associated with the relatively conductive upper-crustal rocks inferred from the determinant resistivity response. Real induction vector and phase-split responses suggest a dominant east-northeast strike at intermediate depth (corresponding to the 5 s response). At greater depth (corresponding to 50 s responses) the dominant geoelectric strike changes from east–east-southeast in the east to southeast in the west. The east–east-southeast geoelectric strike is subparallel to the surface geoelectric boundary and orthogonal to the direction of thrusting of the Kisseynew Belt over the Flin Flon Belt. The different geoelectric strike observed near the west of the Flin Flon Belt is associated with deep structures of the Sturgeon-Weir Thrust and Hanson Lake Block area.

Modelling and interpretation of the Athapapuskow Lake conductivity anomaly

Geoelectric responses

Impedance and induction vector responses from the Athapapuskow area demonstrate that the ALCA can be validly modelled by a 2D structure. The induction vector responses suggest that the ALCA extends for at least 40 km at a strike of ~N25°E (Fig. 6). Multisite, multifrequency Groom–Bailey analysis of sites extending from M09 to M02 indicates a moderately 2D response with regional strike angles of N57°E for the period range 10^{-2}–1 s, and N19°E for the range 1–100 s (Jones and Grant 1997). Considering this information, we adopted a strike of N36°E for modelling the ALCA.

Figure 7 shows the regional TE and TM apparent resistivity and phase pseudosections for the Athapapuskow Lake area, and the ALCA forms a prominent feature in both modes of induction. In apparent resistivity pseudosections, the ALCA forms a region of low resistivity, with values decreasing to <10 Ω·m at periods >1 s. The western edge of ALCA creates a sharp transition in apparent resistivity between sites M09 and M14 and the eastern edge is a more gradual transition near site M01. The phase response is more irregular than the apparent resistivity response, but provides supporting evidence on the form of the ALCA. The phase at periods $<10^{-2}$ s is less than 45°, indicating near-surface rocks are less resistive than those at depth. In the mid-period range, 10^{-2}–10^{2} s, the phase exceeds 45°, indicating an decrease in resistivity with increasing depth. The highest

phases at each period are observed in the area of the ALCA. At long periods the phases decrease, but remain above 45°.

The geoelectric responses (Figs. 6, 7) permit initial qualitative interpretation of the ALCA conductor. The results indicate that the western edge of the structure must be near M14 and may therefore be associated with the ALSZ. The response at site M09 indicates the edge of the conductor lies to the east of the Namew Lake structure. The sharp change in apparent resistivity between M09 and M14, and the real induction vector reversal to the east of this point (at M14 at shorter periods and between M14 and A07 at longer periods) indicate that the conductor dips to the east. Finally, the responses indicate that the structure must include rocks of very low resistivity (<10 Ω·m) and that the integrated conductance through the structure must be considerable.

Two-dimensional modelling and inversion

The approach adopted in the modelling and inversion of the responses sensitive to the presence of the ALCA consisted of preliminary 2D modelling, followed by regularized 2D inversion, and final 2D modelling. In this paper, we describe only the last two steps since they provided the best-fitting and most geologically plausible models. It is important to recognize that the 2D models obtained for the ALCA will represent approximations of the true structure. The geoelectric strikes suggest that the true structure is weakly 3D, with strikes more east–west than N36°E at shallow depths and more north–south at large depths.

2D inversions

The inversion method used in this study was the 2D Occam inversion of deGroot-Hedlin and Constable (1990). The method determines the 2D model that fits the observed data to a specified tolerance and at the same time has minimum roughness, that is, it determines the model that contains the minimum structure required by the data by minimizing the sum of the vertical and horizontal resistivity gradients between each block. The inversion procedure uses the 2D finite-element code of Wannamaker et al. (1987) for its forward response.

Inversions were performed using various combinations of the TE and TM responses and induction vector responses (the component parallel to the profile) from 10 sites in the Athapapuskow Lake area. Prior to the inversions, the local anisotropy in the response at each site was reduced by shifting the TE and TM apparent curves at ~10^{-3} s period to their geometric average value. This process will remove anisotropy for inhomogeneities with a galvanic response at 10^{-3} s. The site gain (intersite static shift) was not removed from the data prior to the inversion. Established methods for its removal, for example., using short- or long-period apparent resistivity values, could not be applied because there are both near-surface and deep structures present along the profile. Considering the residual static shift in the data, the error on the apparent resistivity response was initially set to four times the corresponding error on the phase.

The inversions involved fitting the TE and TM and induction vector responses for 11 periods between 10^{-3} and 10^{2} s. To achieve model convergence from uniform half-space starting models, it was necessary to replace the spectral-based error estimates with larger, synthetic error estimates. The fit to the data at sites near the ALCA was improved by assigning smaller errors for these sites and for the TE mode. Errors for the TM mode were ±3° for the phase, ±0.09 log units for the apparent resistivity (i.e., $\rho_a/1.2 - \rho_a \times 1.2$, equivalent to 20% error), and ±0.15 units for the real and imaginary components of the induction vector. Errors for the TE mode were ±1.5° for the phase, ±0.04 log units for the apparent resistivity, ±0.1 units for the induction vectors. All apparent resistivity and phase errors were decreased by 50% at sites M09, M14, A07, and M08. The resulting model, model B, is shown in Fig. 8.

Examination of the fit to the data of model B reveals that although the model response does not fit the observed data to within the specified limits, it does reproduce most of the major features of the observed response (Fig. 9). The fit to the phase data is relatively good, with the largest misfit occurring at short periods (<10^{-2} s) at sites near the northwestern end of the model. The shape of the model and observed apparent resistivity curves is generally similar, but there is residual static shift in the observed data, for example, at sites M01 and M09. The misfit in the induction vector response is largest for sites M07 and M08. The overall fit to the data could not be improved by inversion of different data sets (individual TE or TM modes, larger or smaller error estimates, no induction vector response), suggesting that much of the misfit can be attributed to minor 3D effects in the observed response. We consider the fit to the data to be sufficiently good that most major features in the inversion model can be interpreted as real components of the true structure. Additional support for this conclusion comes from the fact that these major features also appear in models obtained from inversion of different subsets of the data (not shown here).

The most prominent feature of model B is the southeast-dipping conductor (Fig. 8). At the northwest edge of the conductor, near site M14, its top is located at several kilometres depth; at the southeast edge, near M07, the top is at ~15 km depth. The conductor contains zones in which the resistivity reaches values as low as 5 Ω·m. As these results are for a minimum-structure inversion, the resolved conductor represents the smoothest conductor that could be present in the Earth. The base of the conductor is diffuse: it merges into an underlying region of moderate resistivity, which extends into the lower crust. It is likely that this extended region is an artifact of the minimum-structure inversion. Model B includes relatively resistive upper- crustal blocks at the west and east of the model. The northwestern block has resistivity 500–1000 Ω·m, the southeastern block has resistivity 100–1000 Ω·m, and the base of both blocks dips to the southeast. Model B also includes near-surface resistivity variations including a conductive region near M09 and M14.

Constrained Occam inversion was performed to determine whether the western boundary of the conductor could coincide with the ALSZ. In this test, the ALSZ was introduced as an a priori feature: a resistivity contrast across a 20 km deep, vertical fault, at the location of the ALSZ (several kilometres east of M14), was excluded from the smoothness constraint, thus permitting unpenalized large resistivity contrasts across this boundary. The resulting model (model C, Fig. 8) fitted the data without significant increase in misfit relative to the unconstrained model. The new model includes a strong resistivity contrast across the fault extending from 2

Fig. 7. Pseudosections of the TE and TM response across the ALCA. Contour intervals are the same for TE and TM modes.

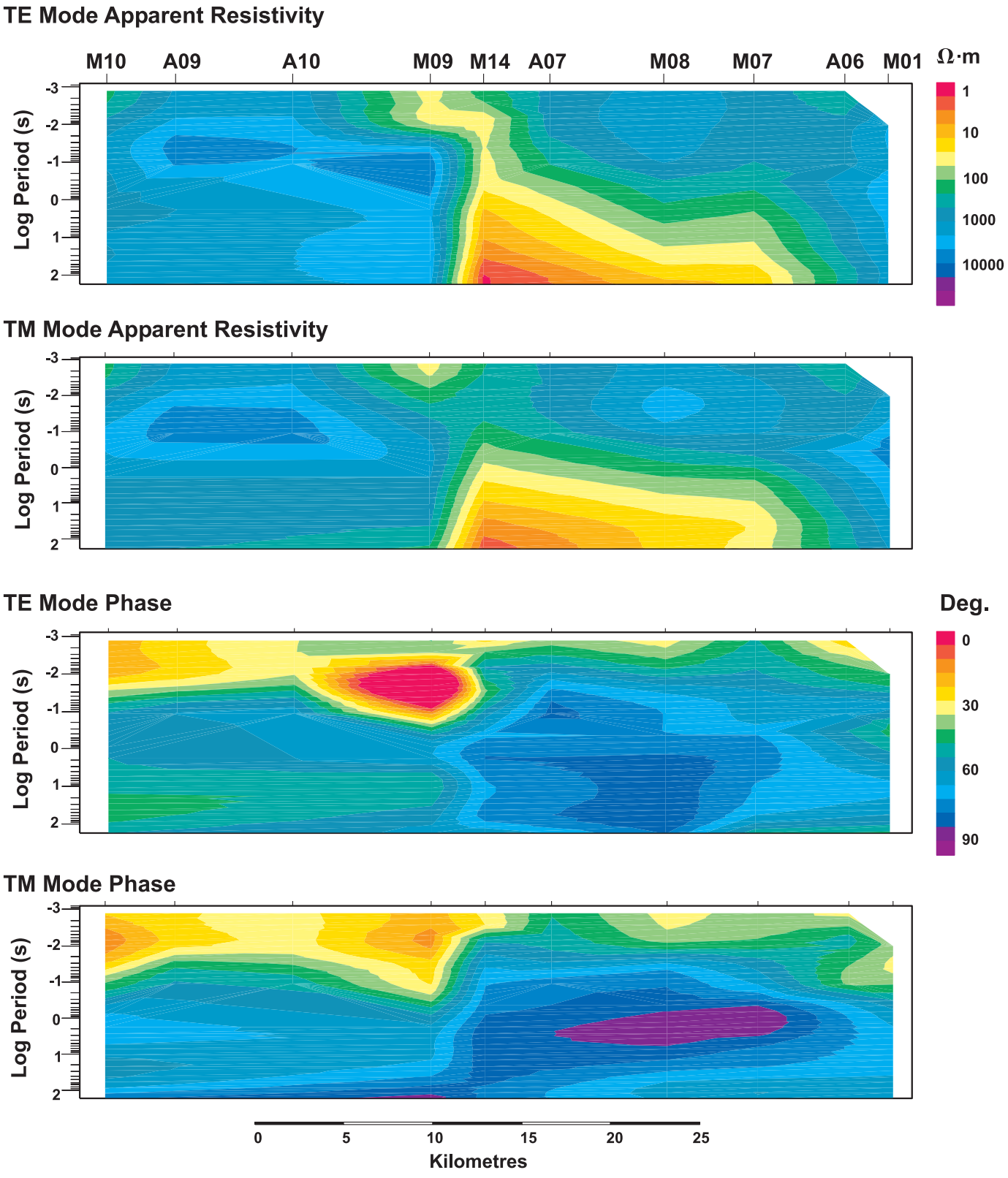

Fig. 8. Two-dimensional resistivity models of the ALCA. (*a*) Minimum-structure inversion models derived from 2D Occam inversion. Model B was obtained using decreased error estimates for the TE mode and for sites M09, M14, A07, and M08; model C was obtained with the ALSZ introduced as an a priori structure. (*b*) Block models derived using forward modelling and simplification of model C. In model D the conductor is represented by a region of uniform resistivity (2 Ω·m); in model E it is represented by a slab of resistivity 1 Ω·m lying within a background zone of resistivity 200 Ω·m.

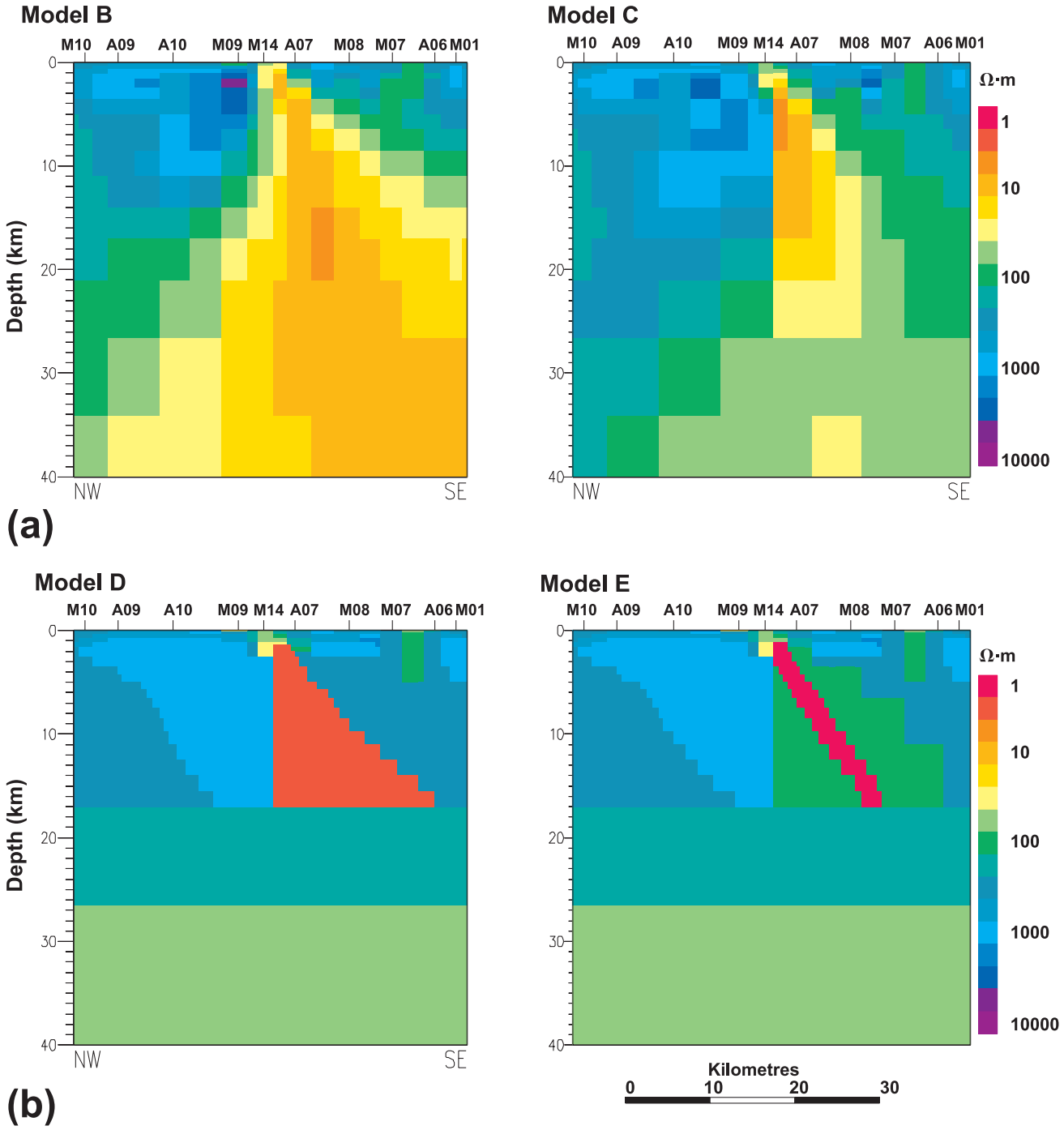

to 20 km depth. To the west of the fault, the resistivity is typically >500 Ω·m, and to the east it is <20 Ω·m. The constrained inversion model again includes a shallow region (<3 km) of relatively low resistivity (5–50 Ω·m) to the northwest of the fault. The inversion results shows the MT response is compatible with a resistivity model in which the ALSZ forms the western margin of the ALCA conductor.

Final 2D forward modelling

The inversion models indicate that the geoelectric response in the Athapapuskow area is due to a southeast-dipping conductor and adjacent resistive blocks. The smooth models are unlikely to have resolved the correct form of the base of the conductor or the underlying resistivity structure, since the MT method usually provides limited resolution of

Fig. 9. Fit to the observed data by model B for the ALCA. Results are shown for the apparent resistivity, impedance phase, and induction vector component parallel to the profile. For the MT plots the circles and solid lines denote the observed and model TE response, and the plus symbols and dashed lines denote the observed and model TM response. For the induction vector plots the circles and solid line denote the observed and model real component and the plus symbols and dashed line the observed and model imaginary component.

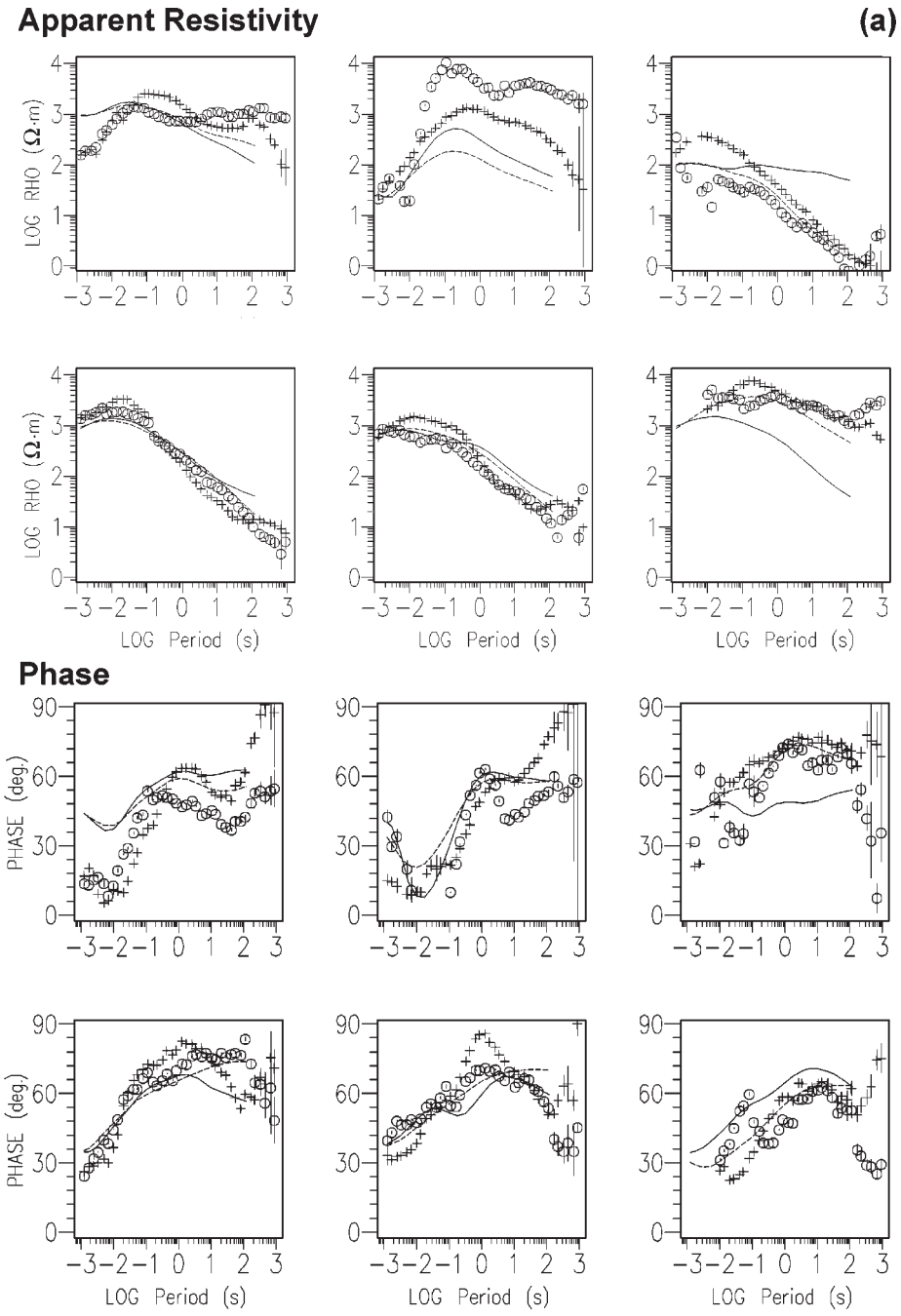

resistive regions below strong conductors (e.g., Ferguson and Edwards 1994). The geoelectric response in the Athapapuskow area could be produced by either a dipping, discrete conductor or a more diffuse conductor as derived by the Occam inversions (Fig. 8, models B and C). Neither the observed apparent resistivity nor the phase response from the area (Fig. 7) provides evidence for resistivity increase beneath the conductor. In the absence of such constraints, minimum-structure inversions will "smear" the low resistivity from a discrete conductor downwards into the underlying region.

Forward modelling was performed to determine whether the ALCA conductor could consist of a more discrete upper-crustal conductor. Inversion model C was "reblocked" into a more discretely parameterized model, and the parameters of the conductor adjusted, in a trial-and-error fashion, until a satisfactory fit to the MT data was obtained. The upper several kilometres of model C was not changed in order to

Fig. 9 (*concluded*).

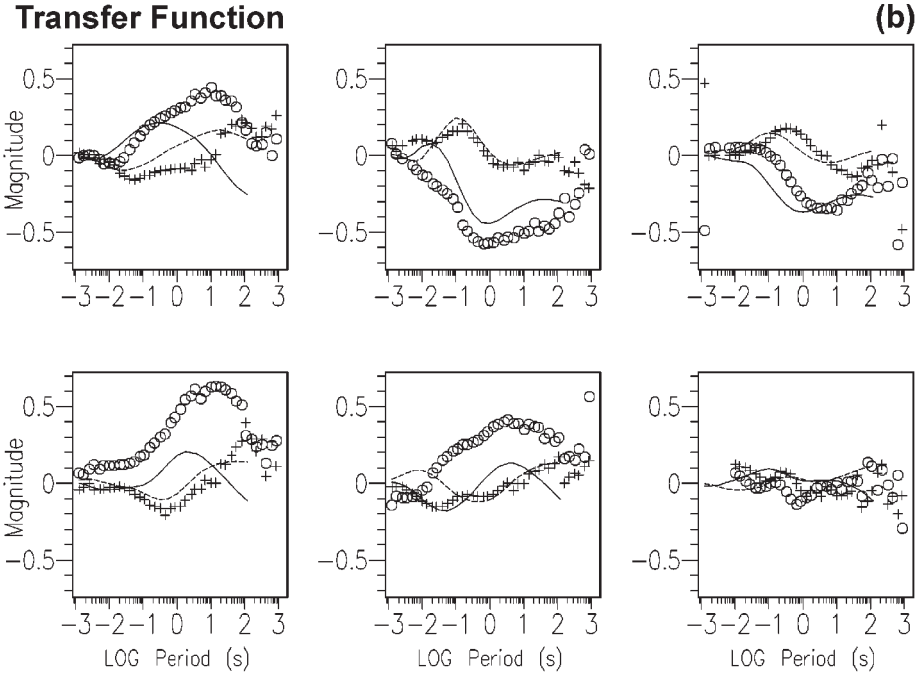

maintain the fit to the short-period data. Figure 8 shows two models (models D and E), representative of a suite of models, that fit the data reasonably well. Both models contain laterally uniform mid- and lower-crustal resistivity (100–500 Ω·m) without the broad conductive zone in the inversion models. In model D, the conductor is represented by a region of uniform resistivity 2 Ω·m, whereas in model E the conductor is represented by a 4–5 km thick slab of resistivity 1 Ω·m lying in a background zone of resistivity 200 Ω·m. The upper-crustal blocks defined in the inversion models are represented in the forward model as 5000 and 1000 Ω·m blocks.

The responses of models D and E are almost identical, indicating that the MT method cannot resolve the exact distribution of conductivity within the gneiss complex. Both models fit the TE response in the vicinity of the conductor better than the inversion models, giving lower apparent resistivity, phase, and induction vector misfits at sites M14 to M07. To define better the structure, a broad range of models was investigated to determine the shared characteristics of models providing a reasonable fit to the data. These characteristics are as follows:

(1) Depth: At its most shallow point (near M14) the top of the conductive body must be at a depth of less than 3 km. The base of the most conductive part of the body must lie between 7 and 9 km depth.

(2) Dip: The top of the body dips to the southeast at an apparent dip angle between 20 and 50°.

(3) Resistivity: The central part of the body has resistivity <2 Ω·m but the body could also include larger zones with resistivity <10 Ω·m.

(4) Thickness and conductance: The thickness of the conductive structure is not resolved: for a 2 Ω·m conductor the body is at least 2 km thick. The integrated conductance (thickness × conductivity) of the ALCA structure must exceed 1000 S.

(5) Shallow conductor: A shallow body with resistivity of <50 Ω·m occurs at the surface near M14 and M09.

Geological interpretation and discussion

Athapapuskow Lake conductor

The MT results show that the ALCA conductor lies in the upper crust and consists of a significant volume of conductive rocks. It extends at least 40 km along strike, is resolved for at least 10 km downdip, and is >2 km thick. The exact spatial distribution of the conductance within the Namew gneiss complex cannot be resolved by the MT data, but the presence of isolated airborne EM anomalies in rocks near the surface suggests the high conductivity is due to a series of discrete conductors. In this situation, model D (Fig. 8) provides an estimate for the bulk or average resistivity of the conductive zone. This average resistivity is 2 Ω·m, so it is probable that the resistivity in the isolated conductors reaches values well under 1 Ω·m.

Based on the interpretation of the seismic data (White et al. 1994; Lucas et al. 1994), the ALCA conductor lies within the Namew gneiss complex. All of the resistivity models (e.g., Fig. 8, models B–E) place the conductor within this gneiss complex. The conductive zone appears to be confined to the western, or structurally lower, part of the gneiss complex. The resistivity of the eastern, or structurally higher, parts of the complex is significantly greater, of order 1000 Ω·m. In models D and E the conductive slab is dipping more steeply than the seismic reflectivity (which dips at 20°). However, the forward modelling results showed that the data can be fitted by a range of models in which the conductor dips at angles between 20 and 50°. It is therefore possible that the conductor dips parallel to the reflectivity.

Crustal conductivity anomalies must be interpreted carefully, since there are a variety of possible sources, including sulphide mineralization, graphitic rocks, and aqueous fluids

(e.g., Jones 1992). However, in the Athapapuskow Lake area the conductor is spatially associated with a geological unit containing numerous drilled airborne EM anomalies, allowing a more reliable interpretation. The probable source of enhanced conductivity in the ALCA conductor is graphitic and sulphidic rocks that occur in pelitic and psammitic gneisses in the subordinate supracrustal subunit of the Namew gneiss complex. Aeromagnetic data interpretations suggest this subunit is more abundant in the east of the Namew gneiss complex (Leclair et al. 1997) where the conductivity is highest. Considering the relative proportion of supracrustal gneisses and ultramafic intrusions within the Namew gneiss complex (Leclair et al. 1993), it is less likely that the source of high conductivity is ultramafic-hosted mineralization as observed at the Namew Lake Ni–Cu mine.

Isotopic and geochemical analyses indicate that the Namew gneiss complex is a mid-crustal equivalent of the Amisk Collage (Leclair et al. 1997). The screens of supracrustal rocks in the gneiss complex are interpreted to be derived from assemblages formed during the period 1.91–1.88 Ga (Lucas et al. 1996; Leclair et al. 1997). The high-grade metamorphism and deformation prevents identification of the specific source of the supracrustal rocks, but the presence of graphite in the pelitic, psammitic, and Ca-rich mafic gneisses supports an intraoceanic origin (Leclair et al. 1993). These results support an oceanic origin for the source rocks of the ALCA.

It is important to consider the formation of the ALCA in terms of the tectonic history in the Namew gneiss complex. The first phase of magmatism recorded in the gneiss complex consisted of intrusion of tonalitic quartz dioritic rocks. U–Pb zircon dating of drill-core samples of quartz diorite gneiss yields an age of 1880 Ma (Leclair et al. 1997). This magmatism was coeval with D_1 deformation and M_1 metamorphism observed in the pyroxenite at Namew Lake mine (Menard et al. 1996). The supracrustal rocks would have been subject to elevated temperatures during the magmatism. Studies of orthogneisses from the Namew mine indicate that temperatures in the igneous rocks initially exceeded 700°C (Cumming and Krstic 1991*a;* Menard et al. 1996). Temperatures easily exceeded the 400–410°C necessary for graphitization to occur (Boerner et al. 1996). The temperature was, in fact, probably sufficiently high to permit oxidation of graphite (e.g., Frost et al. 1989; Hyndman et al. 1993). The presence of graphite in supracrustal gneisses therefore indicates (*i*) that there was either insufficient oxygen for this process to occur, (*ii*) that there was sufficient graphite to buffer the oxygen fugacity, (*iii*) that there was insufficient time for the process to be completed, or (*iv*) that the graphite was reprecipitated from metamorphic or magmatic fluids during the cooling phase (Frost et al. 1989).

The distribution of graphite within the supracrustal rocks may have been affected by later metamorphic events. A second phase of magmatism in the mid-crustal gneiss complex involved intrusion of metre- to kilometre-scale sheets and plutons of granodiorite, tonalite, and diorite. Geochronology, including a date of 1850 ± 2 Ma from a weakly foliated tonalite, suggests this magmatic phase occurred between 1.87 and 1.84 Ga (Leclair et al. 1997). The M_3 metamorphism recorded at the Namew Lake mine, and dated at approximately 1.83 Ga (Menard et al. 1996), is likely related to the magmatism. The amphibolite facies M_3 assemblages in the pyroxenite suggest temperatures of 500–600°C.

Samples drilled from airborne EM anomalies in the Namew gneiss complex have revealed high concentrations of sulphides. The amphibolite-grade metamorphism of the supracrustal rocks probably also involved the concentration and (or) reprecipitation of the sulphides occurring in sulphidic sediments (e.g., Frost and Bucher 1994). Geological and geochemical analysis of the sulphides at the Namew Lake mine indicate mobility and modification of sulphide assemblages throughout the metamorphism (Menard et al. 1996).

The coincidence of the high conductivity and strong seismic reflectivity in the Namew gneiss complex suggests that the two responses may be a result of a common process. Seismic reflectivity in the gneiss complex has been interpreted to be a product of deformation and magmatism occurring between 1.87 and 1.84 Ga (Lucas et al. 1994; Leclair et al. 1997). The conductive components would have been present within the supracrustal rocks and prior to this time (following M_1), but the deformation may be responsible for the morphology and alignment of the conductor. The 1.83 Ga Cormorant Batholith crosscuts the geological fabric in the Namew gneiss complex (Leclair et al. 1993), indicating that the present relationship of supracrustal screens and orthogneisses (and thus conductivity and reflectivity) was established during, or prior to, the deformation.

The resistivity models for the Athapapuskow Lake area include a second region of low resistivity (<50 Ω·m), at shallow depth (<1–2 km) just to the west of the ALSZ (Fig. 9). Because of the relatively broad site spacing, it is impossible to define the exact morphology of this zone, and it is likely that the response is associated with a smaller body of lower resistivity than shown in the models. The low-resistivity region is constrained to lie within the mafic-volcanic Athapapuskow Domain. Leclair et al. (1993) indicate the volcanic package contains electrically conductive zones. It is possible that the conductive zone is associated with the iron formations or shear zones occurring at the western margin of the domain (e.g., Hosain 1984; Syme 1988).

Flin Flon Belt

The MT profile across the Flin Flon Belt provides a sampling of the large-scale geoelectric response of a Palaeoproterozoic greenstone belt. The MT response is characterized by strong galvanic distortion, which can be parameterized statistically by the distribution of shear values (Fig. 5). Overall, the MT distortion within the Palaeoproterozoic rocks of the THO is higher than in the bordering Archaean Superior and Hearne provinces (e.g., Jones and Grant 1997), suggesting that there is an increased abundance of conductive material in the Palaeoproterozoic rocks.

The MT data provide a second image of the ALSZ, approximately 30 km to the west-southwest of the location it was imaged by the seismic reflection survey. Between the two locations the strike of the shear zone changes significantly from north-northeast to east-northeast (Fig. 2). The sharp northwest edge of the ALCA conductor, as well as the pattern of reflection truncations in the seismic data, indicates

that the shear zone maintains a near-vertical dip between the two locations.

The MT response in the north of the Flin Flon Belt provides reasonably strong evidence for a conductive upper crust. Reflection images of this area (line 7a) indicate that there is an east- or east-northeast-dipping detachment at the base of the Flin Flon Belt (event D in Fig. 3*b*) below which there is a relatively reflective zone interpreted as representing highly deformed arc rocks (Lucas et al. 1994). On the basis of both the seismic results and the relatively high conductivity at these depths it is probable that this sequence correlates with the Namew gneiss complex.

The 2D resistivity models in Fig. 8 include an ~5000 Ω·m block in the northwest overlying a region of resistivity ~1000 Ω·m with the base of resistive block dipping to the southeast. This part of the model needs to be interpreted carefully, because the fit of the model response to the observed data is relatively poor for sites M10 and A10 (Fig. 9). However, the model structures are compatible with the structure inferred from the geoelectric strike information, that is, the presence of a more conductive region west of a north-striking conductivity boundary near A08, M10, and M17. The 5000 Ω·m block would therefore correspond to a belt dominated by felsic intrusive rocks, and the adjacent 1000 Ω·m region, to a region of dominantly ocean-floor assemblages.

There are similarities between the electrical resistivity structure in the Trans-Hudson Orogen and in the central Fennoscandian Shield (Korja 1993). In both areas the resistivity of the Archaean and Palaeoproterozoic varies greatly from several thousands of Ω·m to less than 10 Ω·m, and elongated crustal conductors mark major tectonic boundaries. In the Lapland granulite belt, graphite-bearing metasedimentary rocks of the Karasjok-Kittilä greenstone belt exhibit very low resistivity values of <1 Ω·m, comparable to values observed in the ALCA conductor (Korja 1993). The geoelectric structure beneath the Lapland granulite belt also includes dipping conductors that coincide with strong seismic reflections. These dipping conductors are interpreted as being associated with graphite, and possibly to a lesser extent sulphides, in sheared granulites (Korja et al. 1996).

Final interpretation of the conductivity in the Namew gneiss complex requires geochemical and petrophysical analysis of drill-core samples. Aspects requiring investigation include determination of whether the graphite is a product of direct metamorphism of biogenic carbon, precipitation of biogenic graphite remobilized during metamorphism, or precipitation from magmatic fluids. Studies have shown granulite rocks may contain originally biogenic graphite that has been reprecipitated on grain boundaries or in continuous bands (e.g., Mareschal et al. 1994; Korja et al. 1996). In contrast, anomalies with high conductivity attributed to metamorphosed biogenic graphite are observed to extend to moderate depth (e.g., Boerner et al. 1996). The supracrustal rocks of the Namew gneiss complex, which probably reached a metamorphic grade of mid to upper amphibolite facies at the top of the mid-crustal complex, are intermediate between these cases. A second aspect requiring clarification by petrophysical studies is the relative contribution of graphite and sulphides to the conductivity in the Namew gneiss complex. Jones et al. (1996, 1997) show that surface rocks, correlative with the rocks hosting the NACP conductor, have high, but anisotropic, conductivity associated with remobilized sulphides.

Conclusions

Lithoprobe MT surveys in the Palaeoproterozoic Trans-Hudson Orogen in 1992 included 32 sites located in the Flin Flon Belt and adjacent units to the north and south. A significant characteristic of the MT responses across the Flin Flon Belt is strong galvanic distortion. This distortion reflects the complexity of the near-surface geological structure in the greenstone belt and suggests the presence of numerous small-scale structures distributed throughout the upper crust. The results of the survey allow the geoelectric response at sites along the profile line to be divided into four distinct zones:

(1) In the southeast of the survey area, near Cormorant Lake, the geoelectric response is dominated by the contrast between the resistive felsic-intrusive rocks of the Cormorant Batholith and more conductive rocks of the Namew gneiss complex.

(2) In the centre of the profile, the response at sites near Athapapuskow Lake is dominated by a strong upper-crustal conductor.

(3) In the southwest of the survey area, at sites near Amisk Lake, the response is dominated by north–south-striking geoelectric structure. This structure is probably associated with the contrast between felsic-intrusive rocks in the east (Reynard Lake, Kaminis Lake, and Boot–Phantom plutons) and more conductive ocean-floor assemblages (Birch, Sandy Bay, and West Amisk assemblages) to the west.

(4) At sites near the northern boundary of the Flin Flon Belt with the southern flank of the Kisseynew Belt the geoelectric response is related to resistivity structures associated with the boundary. The shorter period (<1 s) responses indicate that the shallow geoelectric structures are aligned with the east–west-striking geological units. At longer periods the geoelectric strike in the east is east–east-southeast, subparallel to the surface geology and orthogonal to the southwest thrusting of the Kisseynew Belt over the Flin Flon Belt. In the northwest of the Flin Flon Belt the geoelectric strike is northwest–southeast and is probably associated with deeper structures of the western Flin Flon Belt, Sturgeon-Weir Thrust, and Hanson Lake Block. The longer period responses indicate the presence of relatively conductive upper-crustal rocks beneath the northern Flin Flon Belt. These are interpreted to correlate with the Namew gneiss complex subcropping south of the belt.

The Lithoprobe MT data provide reasonable resolution of a major conductor in the Athapapuskow Lake area. Modelling of the response reveals that the causitive body dips southeast, with an apparent dip of 20–50°. The MT results constrain the minimum resistivity in the body to be less than 2 Ω·m, the thickness to be at least 2 km, and the conductance to be at least 1000 S. The ALSZ probably forms the sharp western edge of the conductor.

The ALCA conductor lies within the seismically inferred boundaries of the Namew gneiss complex. The MT data cannot resolve the exact distribution of conductance within the complex but, based on airborne EM observations, it is probable that the high conductivity is due to a series of discrete conductors distributed throughout the complex. The conductor is interpreted as being formed by bodies of graphitic and (or) sulphidic, pelitic, and psammitic, supracrustal gneisses that form a subunit of the Namew gneiss complex. A number of airborne EM anomalies in the complex are coincident with sulphidic rocks in this subunit. The shape of the conductor and its coincidence with strong seismic reflectivity is attributed to the mid-crustal structural processes associated with the collisional tectonics between 1.87 and 1.84 Ga.

Acknowledgments

Financial support for this project was provided primarily by the Geological Survey of Canada – Natural Sciences and Engineering Research Council of Canada Lithoprobe project, and also to I.J.F. by University of Manitoba Research grants and a Natural Sciences and Engineering Research Council of Canada operating grant. The data from the contracted MT survey were collected by Phoenix Geophysics, and the staff of Phoenix are thanked for their attention to detail, ensuring high-quality responses. Processing of the LiMS data was performed using software provided by the Geological Survey of Canada and presentation of the results using Geotools. J. Craven, G. McNeice, T. Boyce, C. Farquharson, R. Ellis, and K. Schmigel provided assistance during data acquisition. P. Wannamaker's discussion on lower crustal conductivity on the MTNet Discussion Fora provided an excellent overview of the subject. Critical reviews by S. Lucas, P. Wannamaker, and D. Baird led to significant improvements in the manuscript. This paper was completed while I.J.F. was on study leave at the Geological Survey of Canada and the Department of Exploration Geophysics, Curtin University, Australia.

References

Ansdell, K.M., Lucas, S.B., Connors, K., and Stern, R.A. 1995. Kisseynew metasedimentary gneiss belt, Trans-Hudson orogen (Canada): Back-arc origin and collisional inversion. Geology, **23**: 1039–1043.

Ashton, K.E., and Lewry, J. 1994. Vergence of the "Pelican Slide" and Sturgeon–Weir Shear Zone. Lithoprobe Trans Hudson Orogen Transect 4th Transect Meeting, Lithoprobe Report 38, pp. 12–17.

Ashton, K.E., and Lewry, J. 1996. Geological history of the northern Hanson Lake Block and age relationships between the Pelican décollement zone and Sturgeon-Weir Shear Zone. Lithoprobe Trans Hudson Orogen Transect 6th Transect Meeting, Lithoprobe Report 55, pp. 73–78.

Ashton, K.E., Heaman, L.H., Lewry, J.F., Hartlaub, R.P., and Shi, R. 1999. Age and origin of the Jan Lake Complex: a glimpse at the buried Archean craton of the Trans-Hudson Orogen. Canadian Journal of Earth Sciences, **36**: 185–208.

Boerner, D.E., Kurtz, R.D., and Craven, J.A. 1996. Electrical conductivity and Paleo-Proterozoic foredeeps. Journal of Geophysical Research, **101**: 13 775 – 13 791.

Camfield, P.A., and Gough, D.I. 1977. A possible Proterozoic plate boundary in North America. Canadian Journal of Earth Sciences, **14**: 1229–1238.

Cavaliere, T., and Jones, A.G. 1984. On the identification of a transition zone in electrical conductivity between the lithosphere and asthenosphere: a plea for more precise phase data. Journal of Geophysics, **55**: 23–30.

Chave, A.D., and Smith, J.T. 1994. On electric and magnetic galvanic distortion tensor decompositions. Journal of Geophysical Research, **99**: 4669–4682.

Clowes, R.M. (*Editor*). 1993. Lithoprobe Phase IV proposal—studies of the evolution of a continent. Lithoprobe Secretariat, University of British Columbia, Vancouver, B.C.

Cumming, G.L., and Krstic, D. 1991*a*. Geochronology at the Namew Lake Ni–Cu orebody, Flin Flon area, Manitoba, Canada: thermal history of a metamorphic terrane. Canadian Journal of Earth Sciences, **28**: 309–325.

Cumming, G.L., and Krstic, D. 1991*b*. Geochronology at the Namew Lake Ni–Cu deposit, Flin Flon area, Manitoba, Canada: a Pb/Pb study of whole rocks and ore minerals. Canadian Journal of Earth Sciences, **28**: 1328–1339.

David, J., Bailes, A.H., and Machado, N. 1996. Evolution of the Snow Lake portion of the Paleoproterozoic Flin Flon and Kisseynew belts, Trans Hudson Orogen, Manitoba, Canada. Precambrian Research, **80**: 107–124.

deGroot-Hedlin, C., and Constable, S. 1990. Occam's inversion to generate smooth, two-dimensional models from magnetotelluric data. Geophysics, **55**: 1613–1624.

Fedorowich, J.S., Kerrich, R., and Stauffer, M.R. 1995. Geodynamic evolution and thermal history of the central Flin Flon Domain Trans-Hudson Orogen: Constraints from structural development, $^{40}Ar/^{39}Ar$, and stable isotope geochemistry. Tectonophysics, **14**: 472–503.

Ferguson, I.J., and Edwards, R.N. 1994. Electromagnetic mode-conversion by surface conductivity anomalies: applications for conductivity soundings. Geophysics Journal International, **117**: 48–68.

Frost, B.R., and Bucher, K. 1994. Is water responsible for geophysical anomalies in the deep continental crust? A petrological perspective. Tectonophysics, **231**: 293–309.

Frost, B.R., Fyfe, W.F., Tazaki, K., and Chan, T. 1989. Grain-boundary graphite in rocks and implications for high electrical conductivity in the lower crust. Nature (London), **340**: 134–136.

Gamble, T.D., Goubau, W.M., and Clarke, J. 1979. Magnetotellurics with a remote reference. Geophysics, **44**: 53–68.

Groom, R.W., and Bailey, R.C. 1989. Decomposition of magnetotelluric impedance tensor in the presence of local three-dimensional galvanic distortion. Journal of Geophysical Research, **94**: 1913–1925.

Groom, R.W., and Bailey, R.C. 1991. Analytical investigations of the effects of near-surface three-dimensional galvanic scatterers on MT tensor decomposition. Geophysics, **56**: 496–518.

Groom, R.W., Kurtz, R.D., Jones, A.G., and Boerner, D.E. 1993. A quantitative method to extract regional magnetotelluric impedances and determine the dimension of the conductivity structure. Geophysical Journal International, **115**: 1095–1118.

Hosain, I.T. 1984. Interpretation of airborne magnetic gradiometer surveys of the area south of the Flin Flon – Snow Lake Belt. Manitoba Energy and Mines, Open File Report OF84-2.

Hyndman, R.D., Vanyan, L.L., Marquis, G., and Law, L.K. 1993. The origin of electrically conductive lower continental crust: saline water or graphite?, Physics of the Earth and Planetary Interiors, **81**: 325–344.

Jones, A.G. 1988. Static shift of magnetotelluric data and its removal in a sedimentary basin environment. Geophysics, **53**: 967–978.

Jones, A.G. 1992. Electrical conductivity of the lower continental crust. Chapter 3. *In* Continental lower crust. *Edited by* D. Fountain, R.J. Arculus, and R.W. Kay. Elsevier, Amsterdam, pp. 81–143.

Jones, A.G. 1993. Electromagnetic images of modern and ancient subduction zones. *In* Plate tectonic signatures in the continental lithosphere. *Edited by* A.G. Green, A. Kroener, H.-J. Goetze, and N. Pavlenkova. Tectonophysics, **219**: 29–45.

Jones, A.G., and Grant, N.J. 1997. Geoelectric strike directions for the 1992 THOT MT data. Report of Lithoprobe Trans Hudson Orogen Transect 7th Transect Meeting, Saskatoon.

Jones, A.G., and Jodicke, H. 1984. Magnetotelluric transfer function estimation improvement by a coherence-based rejection technique. 54th Society of Exploration Geophysics Meeting, Atlanta, Georgia, Expanded Abstracts, pp. 51–55.

Jones, A.G., Chave, A.D., Auld, D., Bahr, K., and Egbert, G. 1989. A comparison of techniques for magnetotelluric response function estimation. Journal of Geophysical Research, **94**: 14 201 – 14 213.

Jones, A.G., Kurtz, R.D., Craven, J.A., McNeice, G.W., Gough, D.I., DeLaurier, J.M., and Ellis, R.G. 1992. Electromagnetic constraints on strike-slip fault geometry—The Fraser River fault system. Geology, **20**: 561–564.

Jones, A.G., Craven, J.A., McNeice, G.W., Ferguson, I.J., Boyce, T.T., Farquharson, C., and Ellis, R. 1993. North American Central Plains conductivity anomaly within the Trans-hudson orogen in northern Saskatchewan, Canada. Geology, **21**: 1027–1030.

Jones, A.G., Katsube, J., and Ferguson, I.J. 1996. Palaeoproterozoic tectonic processes revealed through electromagnetic studies of the North American Central Plains (NACP) conductivity anomaly: from continental to hand sample scale. 66th Society of Exploration Geophysics Meeting, Denver, Colorado.

Jones, A.G., Katsube, T.J., and Schwann, P. 1997. The longest conductivity anomaly in the world explained: sulphides in fold hinges causing very high electrical anisotropy. Journal of Geomagnetism and Geoelectricity, **49**: 1619–1629.

Jones, F.W., and Correia, A. 1992. Magneto-telluric soundings in the frequency range 0.01–130 Hz in northern Saskatchewan. Report of Lithoprobe Trans Hudson Orogen Transect 2rd Transect Meeting, Saskatoon.

Jones, F.W., and Kalvey, A. 1993. Magnetotelluric measurements between 106°–107° W and 55.5°–55.75° N in northern Saskatchewan. Report of Lithoprobe Trans Hudson Orogen Transect 3rd Transect Meeting, Regina.

Korja, T. 1993. Electrical conductivity distribution of the lithosphere in the central Fennoscandian Shield. Precambrian Research, **64**: 85–108.

Korja, T., Tuiska, P., Pernu, T., and Karhu, J. 1996. Field, petrophysical and carbon isotope studies on Lapland granulite belt: implications for deep continental crust. Terra Nova, **8**: 48–58.

Leclair, A.D., Scott, R.G., and Lucas, S.B. 1993. Sub-Palaeozoic geology of the Flin Flon Belt from integrated drillcore and potential field data, Cormorant Lake area, Manitoba and Saskatchewan, *In* Current research, part C. Geological Survey of Canada, Paper 93-1C, pp. 249–258.

Leclair, A.D., Lucas, S.B., and Stern, R.A. 1994. Tectonics of the Flin Flon – Snow Lake Belt: view from below the Phanerozoic cover. Lithoprobe Trans Hudson Orogen Transect 4th Transect Meeting, Lithoprobe Report 38, pp. 123–134.

Leclair, A.D., Lucas, S.B., Broom, H.J., Viljoen, D.W., and Weber, W. 1997. Regional mapping of Precambrian basement beneath Phanerozoic cover in southeastern Trans-Hudson Orogen, Manitoba and Saskatchewan. Canadian Journal of Earth Sciences, **34**: 618–634.

Lewry, J.F., and Collerson, K.D. 1990. The Trans Hudson Orogen: extent, subdivision, and problems. *In* The Early Proterozoic Trans Hudson Orogen of North America. *Edited by* J.F. Lewry and M.R. Stauffer. Geological Association of Canada, Special Paper 37, pp. 1–14.

Lucas, S.B., White, D., Hajnal, Z., Lewry, J., Green, A., Clowes, R., Zwanzig, H., Ashton, K., Schledewitz, D., Stauffer, M., Norman, A., Williams, P.F., and Spence, G. 1994. Three-dimensional collisional structure of the Trans Hudson Orogen, Canada. Tectonophysics, **232**: 161–178.

Lucas, S.B., Stern, R.A., Syme, E.C., Reilly, B.A., and Thomas, D.J. 1996. Intraoceanic tectonics and the development of continental crust: 1.92–1.84 Ga evolution of the Flin Flon Belt, Canada. Geological Society of America Bulletin, **108**: 602–629.

Mareschal, M., Kurtz, R.D., and Bailey, R.C. 1994. A review of electromagnetic investigations in the Kapuskasing uplift and surrounding regions: electrical properties of key rocks. Canadian Journal of Earth Sciences, **31**: 1042–1051.

Maxeiner, R.O., Sibbald, T.I.I., Slimmon, W.L., Heaman, L.M., and Watters, B.R. 1999. Lithogeochemistry of volcano-plutonic assemblages of the southern Hanson Lake Block and southeastern Glennie Domain, Trans-Hudson Orogen: evidence for a single island arc complex. Canadian Journal of Earth Sciences, **36**: 209–225.

McNeice, G., and Jones, A.G. 1996. Multisite, multifrequency tensor decomposition of magnetotelluric data. 66th Society of Exploration Geophysics Meeting, Denver, Colorado, Expanded Abstracts, **66**: 281–284.

Menard, T., Lesher, C.M., Stowell, H.H., Price, D.P., Pickell, J.R., Onstott, T.C., and Hulbert, L. 1996. Geology, genesis, and metamorphic history of the Namew Lake Ni–Cu deposit, Manitoba. Economic Geology, **91**: 1394–1413.

Syme, E.C. 1988. Athapapuskow Lake project. Manitoba Energy and Mines, Report of Activities, pp. 20–34.

Truman, E. 1992. Stake a claim in Manitoba: Flin Flon – Snow Lake area, 1 : 250,000 mineral deposit and property holder map. Manitoba Energy and Mines, Winnipeg.

Unsworth, M.J., Malin, P., Egbert, G.D., and Booker, J.R. 1997. Internal structure of the San Andreas fault at Parkfield, California. Geology, **25**: 359–362.

Vozoff, K. 1991. The magnetotelluric method. *In* Electromagnetic methods in applied geophysics. Vol. 2. Applications. *Edited by* M.N. Nabighian. Society of Exploration Geophysicists, Tulsa, OK, pp. 641–711.

Wannamaker, P.E., Stodt, J.A., and Rijo, L. 1987. A stable finite-element solution for two-dimensional magnetotelluric modelling, Geophysics, **88**: 277–296.

White, D.J., Lucas, S.B., Hajnal, Z., Green, A.G., Lewry, J.F., Weber, W., Bailes, A.H., Syme, E.C., and Ashton, K. 1994. Paleo-Proterozoic thick-skinned tectonics: Lithoprobe seismic reflection results from the eastern Trans-Hudson Orogen. Canadian Journal of Earth Sciences, **31**: 458–469.

White, D., Boerner, D., Wu, J., Lucas, S., Berrer, E., Hannila, J., and Somerville, R. 1996. Seismic reflection and electromagnetic investigations of the Thompson Nickel Belt. Lithoprobe Trans Hudson Orogen Transect, 6th Annual Meeting, Saskatoon.

White, D.J., Boerner, D.E., Wu, J., Lucas, S.B., Berrer, E., Hannila, J., and Somerville, R. 1997. High -resolution seismic and controlled-source EM studies near Thompson, Manitoba. *In* Proceedings of Exploration 97: 4th Decennial International Conference on Mineral Exploration. *Edited by* A.G. Gubins. Paper 87, pp. 685–694.

White, D.J., Jones, A.G., Lucas, S., and Hajnal, Z. 1999. Tectonic evolution of the Superior Boundary Zone from coincident seismic reflection and magnetotelluric profiles. Tectonics, **18**: 430–451.

Zhang, P., Pedersen, L.B., Mareschal, M., and Chouteau, M. 1993. Channelling contribution to tipper vectors: a magnetic equivalent to electrical distortion, Geophysical Journal International, **113**: 693–700.